

RESEARCH

Open Access



# ALS-linked mutant TDP-43 in oligodendrocytes induces oligodendrocyte damage and exacerbates motor dysfunction in mice

Mai Horiuchi<sup>1,2†</sup>, Seiji Watanabe<sup>1,2†</sup>, Okiru Komine<sup>1,2</sup>, Eiki Takahashi<sup>3</sup>, Kumi Kaneko<sup>4</sup>, Shigeyoshi Itoharu<sup>5</sup>, Mayuko Shimada<sup>6,7</sup>, Tomoo Ogi<sup>6,7</sup> and Koji Yamanaka<sup>1,2,8,9,10\*</sup> 

## Abstract

Nuclear clearance and cytoplasmic aggregation of TAR DNA-binding protein of 43 kDa (TDP-43) are pathological hallmarks of amyotrophic lateral sclerosis (ALS) and its pathogenic mechanism is mediated by both loss-of-function and gain-of-toxicity of TDP-43. However, the role of TDP-43 gain-of-toxicity in oligodendrocytes remains unclear. To investigate the impact of excess TDP-43 on oligodendrocytes, we established transgenic mice overexpressing the ALS-linked mutant TDP-43<sup>M337V</sup> in oligodendrocytes through crossbreeding with *Mbp-Cre* mice. Two-step crossbreeding of floxed TDP-43<sup>M337V</sup> and *Mbp-Cre* mice resulted in the heterozygous low-level systemic expression of TDP-43<sup>M337V</sup> with (Cre-positive) or without (Cre-negative) oligodendrocyte-specific overexpression of TDP-43<sup>M337V</sup>. Although Cre-negative mice also exhibit subtle motor dysfunction, TDP-43<sup>M337V</sup> overexpression in oligodendrocytes aggravated claspings signs and gait disturbance accompanied by myelin pallor in the corpus callosum and white matter of the lumbar spinal cord in Cre-positive mice. RNA sequencing analysis of oligodendrocyte lineage cells isolated from whole brains of 12-month-old transgenic mice revealed downregulation of myelinating oligodendrocyte marker genes and cholesterol-related genes crucial for myelination, along with marked upregulation of apoptotic pathway genes. Immunofluorescence staining showed cleaved caspase 3–positive apoptotic oligodendrocytes surrounded by activated microglia and astrocytes in aged transgenic mice. Collectively, our findings demonstrate that an excess amount of ALS-linked mutant TDP-43 expression in oligodendrocytes exacerbates motor dysfunction in mice, likely through oligodendrocyte dysfunction and neuroinflammation. Therefore, targeting oligodendrocyte protection, particularly through ameliorating TDP-43 pathology, could represent a potential therapeutic approach for ALS.

**Keywords** Amyotrophic lateral sclerosis, TDP-43, Oligodendrocyte, Myelin, Apoptosis, Neuroinflammation, Animal model, Behavioral test, RNA-sequencing

<sup>†</sup>Mai Horiuchi and Seiji Watanabe have contributed equally to this work.

\*Correspondence:

Koji Yamanaka

[yamanaka.koji.p4@f.mail.nagoya-u.ac.jp](mailto:yamanaka.koji.p4@f.mail.nagoya-u.ac.jp)

Full list of author information is available at the end of the article



## Introduction

Amyotrophic lateral sclerosis (ALS) is a progressive, fatal neurodegenerative disease characterized by selective degeneration of upper and lower motor neurons [60]. Despite being described over 150 years ago, effective treatments have not been developed. Approximately 90% of ALS cases are sporadic ALS (sALS), with the remaining cases being familial ALS (fALS). More than 30 genes have been identified as ALS-causative genes, including *TARDBP*, *C9orf72*, *TBKI*, *FUS*, and *OPTN*, which are also implicated in frontotemporal lobar degeneration (FTLD) [19].

TAR DNA-binding protein of 43 kDa (TDP-43), an RNA/DNA-binding protein encoded by *TARDBP*, is involved in ALS pathogenesis [10, 50]. Over 50 mutations in *TARDBP* are associated with ALS and/or FTLD, and ALS caused by *TARDBP* mutations is defined as ALS10 [57, 65, 74]. TDP-43 plays multiple roles in mRNA metabolism, including transcription, translation, splicing, and mRNA stabilization, through direct binding to >6000 mRNAs [35, 49, 61]. Under normal conditions, TDP-43 predominantly localizes in the nucleus, whereas in ALS, it mislocalizes in the cytoplasm, forming insoluble aggregates with ubiquitination and phosphorylation, referred to as TDP-43 pathology [2, 37]. This pathology is a common feature in both fALS and sALS, being present in >95% of all ALS cases, regardless of TDP-43 mutations [35, 59]. Therefore, understanding how aberrant TDP-43 protein leads to neurodegeneration is crucial.

Various rodent studies have revealed that TDP-43 pathology manifests as loss-of-function and/or gain-of-toxicity phenotypes, i.e., loss of its nuclear function and cytoplasmic toxicity from TDP-43 aggregates, respectively (Additional file 4: Fig. S1) [10]. In ALS, TDP-43 inclusions are primarily found in motor neurons and oligodendrocytes in ALS [38, 54]. Studies have shown that motor neuron-specific deletion or neuronal overexpression of TDP-43 in rodents results in severe motor dysfunction and motor neuron damage [12, 24, 28], implicating both TDP-43 loss-of-function and gain-of-toxicity mechanisms. There is limited information regarding the pathomechanisms of TDP-43 in oligodendrocytes. Oligodendrocytes, which produce myelin to enable saltatory conduction and provide metabolic support to axons [34], are critical for maintaining neuronal function. Oligodendrocyte dysfunction is also noted as a pathological feature of ALS [16, 34, 41, 48], with demyelination reported in the motor cortices, ventral horn gray matter, and lateral corticospinal tract of the lumbar spinal cord in patients with ALS [30]. In a mutant SOD1-ALS mouse model, oligodendrocytes derived from oligodendrocyte precursor cells (OPCs) lose myelination capability [48], whereas selective mutant SOD1 deletion

in OPCs delays disease onset and extends survival [30]. Moreover, TDP-43 pathology appears in oligodendrocytes in the gray matter of the ventral spinal cord in the early stage of ALS, before neuronal inclusion formation [5]. Collectively, these findings indicate that TDP-43 pathology in oligodendrocytes may accelerate ALS progression by compromising oligodendrocyte function.

Previous research has revealed that TDP-43 binds to mRNAs of myelination-related genes, including *Mbp*, which encodes myelin basic protein (MBP), and that oligodendrocyte-specific TDP-43 deletion impairs myelination, causing severe motor dysfunction and reduced survival in mice with oligodendrocyte necroptosis [67]. TDP-43 plays an important role in maintaining the homeostasis of OPCs and myelinating oligodendrocytes [22]. Additionally, TDP-43 regulates cholesterol metabolism in oligodendrocytes [23]. These studies emphasize the essential role of TDP-43 in oligodendrocyte function. Despite these findings, the precise mechanism underlying gain-of-toxicity of TDP-43 in oligodendrocytes has not been investigated. In the present study, to unravel the effect of excess TDP-43 in oligodendrocytes, we generated and analyzed the mouse model overexpressing ALS-linked TDP-43<sup>M337V</sup> in oligodendrocytes.

## Materials and methods

### Animals

To establish a mouse model for conditional expression of the ALS-linked TDP-43<sup>M337V</sup> mutant [B6-Gt(ROSA)26Sor<tm(CAG-TARDBP\*M337V)>; hTDP-43<sup>M337V</sup>-cTg], a gene-targeting vector carrying the mutant *Rosa26* locus was created as follows. DNA fragments of the cytomegalovirus enhancer/chicken  $\beta$ -actin promoter from the pCAGGS [39] vector, the woodchuck hepatitis virus posttranscriptional regulatory element, and the gene cassette of a neomycin resistance gene controlled by the phosphoglycerate kinase I promoter (PGK-Neo<sup>r</sup>) and polyA sequences flanked by the loxP sequences (PGK-Neo<sup>r</sup>-4xPA-flox) were sequentially cloned into the pRosa26-1 vector (a kind gift from Dr. P. Soriano) [56]. Subsequently, human TDP-43<sup>M337V</sup> cDNA was inserted into the XhoI site of pRosa26-1 to complete construction of the gene-targeting vector. Targeted gene insertion was performed using embryonic stem (ES) cells derived from 129/Ola mice. Correctly targeted ES cells were microinjected into C57BL/6J mouse blastocysts to generate chimeric embryos. Mice carrying the heterozygous TDP-43<sup>M337V</sup> mutant allele (hTDP-43<sup>M337V</sup>-fl/wt) were backcrossed to C57BL/6J mice and maintained in a C57BL/6J genetic background. FVB/N-Tg(Mbp-cre)9Gvn/Gvn-Rbrc mice (*Mbp-Cre* mice, RBRC01461) [40] were obtained from RIKEN BioResource Research Center (Ibaraki, Japan). *Mbp-Cre* mice were crossbred with

homozygous hTDP-43<sup>M337V</sup>-fl/fl mice to obtain *Mbp-Cre*<sup>+</sup>; hTDP-43<sup>M337V</sup>-fl/wt mice, and these mice were further crossed with hTDP-43<sup>M337V</sup>-fl/fl mice. Littermates resulting from this crossbreeding were used in this study to minimize genetic background variability introduced by *Mbp-Cre* mice. B6.129P2-Gt(ROSA)26Sor<tm1(NLS-lacZ)Ito mice (*Rosa-NLS-LacZ* mice, RBRC02657) [32] were crossed with *Mbp-Cre* mice to confirm the cell-type specificity of Cre mediated-recombination. All mice were housed under specific pathogen-free conditions (12/12 h light–dark-cycle; 23 °C ± 1 °C; 50% ± 5% humidity) and handled according to the Animal Care and Use Committee guidelines of Nagoya University and RIKEN. Primer sequences used for genotyping polymerase chain reaction (PCR) are listed in Additional file 1: Table S1A.

### Behavioral tests

Hindlimb clasping was scored on a scale from 0 (normal) to 3 (fully retracted) during a 10-s observation, as described previously [20]. The balance beam test was performed according to the protocol modified from previous studies [64]. Mice weighing over 40 g were excluded from the analysis. Briefly, a 24-mm-wide beam and a goal box were installed 55 cm above the floor. Mice were placed in a darkened goal box for 2 min and then trained to cross the beam four times toward the goal box, which was placed 60 cm from the start line. Following training, mice crossed both 24- and 14-mm-wide beam three times. Between trials, mice rested in the goal box for 60 s. Videos of the trials were used to measure total crossing time, total steps, and hindlimb slips. The means of these measurements were plotted on graphs.

For rotarod tests, mice were placed on rotating rods accelerating from 0 to 30 rpm for 5 min at 15-min intervals between each trial (Muromachi Kikai, Tokyo, Japan). The longest latency to fall from the rotating rods from three trials was recorded.

Stride length was measured by recording mice walking on a transparent acrylic board from below using a handheld video recorder. GIMP 2.10.34 software (<https://www.gimp.org>) were used to measure left and right hindlimb stride length from screenshots of the videos. Means of 10 measurements were plotted on graphs.

The forelimb and hindlimb grip strengths were measured using a grip strength meter (Muromachi Kikai). The forepaws or hindpaws of the mice were placed on a bar or grid, respectively, and their tails were gently pulled back by the examiner. The grip strengths (kgf) were recorded, omitting the highest and lowest scores from five consecutive trials. The means of three scores was plotted on a graph. All tests were performed every 1.5 months without randomization or blinding.

### Antibodies

The antibodies used in this study were as follows: mouse monoclonal anti-Myc-Tag (9B11) (1:1000 for immunoblotting, 1:500 for immunofluorescence; #2276S, Cell Signaling Technology, Danvers, MA, USA), mouse monoclonal anti-TDP-43 (3H8) (1:1000; #MABN45, Merck Millipore, Burlington, MA, USA), mouse monoclonal anti-β-actin (1:5000; #A5441, Sigma-Aldrich, St. Louis, MO, USA), goat polyclonal anti-PDGFRα (1:200; #AF1062, R&D Systems, Minneapolis, MN, USA), mouse monoclonal anti-APC (cc-1) (1:500; #OP80, Merck Millipore), rabbit polyclonal anti-Myc-Tag (1:500; #562, Medical & Biological Laboratories, Tokyo, Japan), goat polyclonal anti-AIF-1/Iba1 (1:250; #NB100-1028, Novus Biologicals, Littleton, CO, USA), mouse monoclonal anti-GFAP (1:500; #G3893, Sigma-Aldrich), rabbit polyclonal anti-Iba1 (1:500; #019-19741, Wako, Osaka, Japan), rabbit polyclonal anti-GFAP (1:200; #MSFR101830, Nittobo Medical, Tokyo, Japan), rabbit polyclonal anti-TDP-43 (1:500; #10782-2-AP, Proteintech, Rosemont, IL, USA), goat polyclonal anti-Choline Acetyltransferase (1:100; #AB144P, Sigma-Aldrich), rabbit polyclonal anti-Cleaved Caspase-3 (Asp175) (1:200; #9661, Cell Signaling Technology), rat monoclonal anti-Mac2 (1:500; #CL8942AP, Cedarlane Laboratories, Burlington, Canada), mouse monoclonal anti-b-Galactosidase (1:300; #Z3781, Promega, Madison, WI, USA), rabbit polyclonal anti-Olig2 (1:500; #AB9610, Merck Millipore), rabbit monoclonal anti-Mbp (1:1000; #ab218011, Abcam), rabbit polyclonal anti-Mbp (1:200; #AB980, Merck Millipore), rat monoclonal anti-CD16/CD32 (1:250; #14-0161-82, Thermo Fisher Scientific, Waltham, MA, USA), and mouse monoclonal anti-O1 (1:50; #MAB344, Merck Millipore). Alexa Fluor–conjugated and horseradish peroxidase (HRP)-conjugated secondary antibodies were purchased from Thermo Fisher Scientific and Jackson ImmunoResearch Laboratories (West Grove, PA, USA).

### Immunoblotting

Mice were deeply anesthetized and transcardially perfused with phosphate-buffered saline (PBS) for 5–10 min. The corpus callosum or lumbar spinal cord was sonicated in ice-cold radioimmunoprecipitation assay buffer [25 mM Tris-HCl (pH 7.4), 150 mM NaCl, 1% (v/v) Nonidet P-40 (Sigma-Aldrich), and 0.5% (w/v) sodium deoxycholate (Sigma-Aldrich)] supplemented with protease and phosphatase inhibitor cocktails (both from Roche, Basel, Switzerland). Lysates were centrifuged at 10,000×g and 4°C for 5 min, and the supernatants were collected. Protein concentration in the supernatants was measured using a Bradford Protein Assay Kit (Bio-Rad Laboratories, Richmond, CA, USA). Equal amounts of protein

were mixed with 6×sodium dodecyl sulfate (SDS)–polyacrylamide gel electrophoresis (PAGE) loading buffer [125 mM Tris-HCl (pH 6.8), 4% (w/v) SDS, 10% (v/v) glycerol, and 0.04% (w/v) bromophenol blue] containing 2.5% (v/v) 2-mercaptoethanol and incubated for 3 min at 95°C. Samples were subjected to SDS-PAGE and transferred to a polyvinylidene fluoride membrane (Immobilon-P, Merck Millipore). The membrane was incubated with blocking buffer [25 mM Tris-HCl (pH 7.4), 150 mM NaCl, 0.05% (v/v) Tween-20, and 2% (w/v) bovine serum albumin (BSA; Nacalai Tesque, Kyoto, Japan)] and then further incubated overnight with primary antibodies at 4°C, followed by incubation with secondary antibodies. Primary and secondary antibodies were diluted with blocking buffer and Tris-buffered saline (TBS), respectively. Bound secondary antibodies were visualized using Immobilon Crescendo Western HRP Substrate (Merck Millipore), and images were captured using a LAS-4000 mini system (Fujifilm) with Multi-Gauge software (Fujifilm).

#### Immunofluorescence

Mice were deeply anesthetized and then transcardially perfused with PBS for 5 min followed by 4% (w/v) paraformaldehyde in 0.1 M phosphate buffer for 10 min. After overnight postfixation in paraformaldehyde/phosphate buffer, the spinal cords and brains of mice were dissected and transferred to 30% (w/v) sucrose in PBS for cryoprotection. Tissues were incubated for more than 3 days, embedded in Tissue-Tek OCT compound medium (Sakura Fine, Tokyo, Japan), and were frozen at –80°C until use. Tissue Sects. (30- $\mu$ m sections of the brain or 12- $\mu$ m sections of the lumbar spinal cord) produced using a cryostat (Leica Biosystems, Wetzlar, Germany) were permeabilized with 0.5% (w/v) Triton X-100 in PBS for 30 min and incubated in blocking buffer [5% (v/v) normal serum and 0.3% (w/v) Triton X-100 in PBS] for 60 min. Following blocking, sections were incubated overnight with primary antibodies at 4°C, followed by incubation with secondary antibodies. For Myc-Tag (9B11) staining, 12- $\mu$ m spinal cord sections were mounted on glass microscope slides, and TBS was used instead of PBS. Primary and secondary antibodies were diluted with blocking buffer. Sections were mounted using Fluoromount/Plus (Diagnostic BioSystems, CA, USA), and images were acquired using confocal laser scanning microscopy (LSM-700 or LSM-900; Carl Zeiss AG, Oberkochen, Germany) with Zen software (Carl Zeiss). Fluorescence intensities were quantified using ImageJ (<https://imagej.net/ij/>).

#### Woelcke staining

Brain or lumbar spinal cord tissues from mice embedded in Tissue-Tek OCT compound medium were sectioned at 20  $\mu$ m using a cryostat and placed on microscope slides. The slides were incubated in 70% (v/v) ethanol for 2 h at room temperature, followed by washing in distilled water. Subsequently, the slides were incubated overnight at room temperature in 2.5% (w/v) ferric ammonium sulfate (Kanto Chemical, Tokyo, Japan) in distilled water. After further washing in distilled water, the slides were incubated in a staining solution [10% (v/v) ethanol, 0.5% (w/v) hematoxylin hydrate (Tokyo Chemical Industry, Tokyo, Japan), and 0.067% (w/v) lithium carbonate (Kanto Chemical)] for approximately 3 h. Following additional washes in distilled water, slides were subsequently incubated in 70% (v/v) ethanol, 99.5% (v/v) ethanol, and xylene for 10 min each. Finally, the sections were mounted using Permount (FALMA, Tokyo, Japan). Staining intensities were quantified using ImageJ.

#### Isolation of oligodendrocyte lineage cells from the mouse brain

Mice were deeply anesthetized and transcardially perfused with PBS for 5 min. Whole brains were collected in gentleMACS™ C Tubes (Miltenyi Biotec, Bergisch-Gladbach, Germany) and minced with scissors in preheated dissociation buffer (Neural Tissue Dissociation Kit-Postnatal Neurons, Miltenyi Biotec). The C Tubes were placed on a gentleMACS™ dissociator (Miltenyi Biotec), and the tissues were dissociated into single-cell suspensions for 30 min at 37°C. The cell suspensions were passed through 70- $\mu$ m cell strainers (pluriSelect Life Science, Leipzig, Germany) with 0.5% (w/v) BSA (Nacalai Tesque) in PBS using the plungers of 5-mL syringes and centrifuged at 600×g, and room temperature for 5 min. After aspirating the supernatant, the cell suspensions were mixed with 40% (v/v) Percoll™ (Cytiva Sweden AB, Uppsala, Sweden) in PBS and centrifuged at 620×g at room temperature for 25 min. Debris and supernatant were removed, and the suspensions were incubated with anti-CD16/CD32 antibodies (1:250 in PBS for Fc receptor blocking) and O1-antibody (1:50 in PBS) at 4°C for 10 and 20 min, respectively. After washing with BSA/PBS, magnetic beads [anti-mouse IgM MicroBeads (1:10, #130-047-301, Miltenyi Biotec), CD140a (PDGFR $\alpha$ ) MicroBead Kit (1:10; #130-101-502, Miltenyi Biotec), and anti-O4 MicroBeads (1:40; #130-094-543, Miltenyi Biotec)] were added to the suspensions and incubated at 4°C for 15 min. Oligodendrocyte lineage cells bound to magnetic beads were isolated via magnetic-activated cell sorting (MACS) using the autoMACS Pro Separator (Miltenyi Biotec).

### RNA sequencing experiments

For the RNA-sequencing (RNA-seq), oligodendrocyte lineage cells were isolated from the whole brains of non-transgenic and *Mbp-Cre<sup>+</sup>*; hTDP-43<sup>M337V</sup>-fl\*/fl mice at 12 months of age (n=3 per mouse type). Total RNA was extracted from MACS-isolated oligodendrocyte lineage cells using the RNeasy Micro Kit (Qiagen, Hilden, Germany) according to the manufacturer's instructions. RNA concentrations and quality were measured using an Agilent 2100 Bioanalyzer (Agilent Technologies, Santa Clara, CA, USA). The RNA integrity number of the samples was >7.7. Libraries were prepared using the NEBNext Poly mRNA Magnetic Isolation Module (New England Biolabs, MA, USA) for mRNA isolation and the MGI Easy RNA Directional Library Prep Set (MGI, Shenzhen, China). Subsequently, 151-nt paired-end reads were sequenced on the DNBSEQ-G400RS sequencer (MGI).

### RNA-seq data analysis

Adapter sequences and low-quality bases (quality score < 20) were trimmed from the 3'-ends of the sequencing reads using fastp v0.23.2 [8, 9]. Reads were quality checked using fastp v0.23.2 before and after trimming. The trimmed reads were aligned to the mouse genome version mm10 assembly using HISAT2 v2.2.1 [31], with strand specificity information employed for reads prepared using the standard kit. Alignments to rDNA regions were excluded using BEDTools v2.25.0 [52]. The expression levels of individual annotated genes were quantified from the mapping data using StringTie v2.2.1 [47]. Gene count matrices were generated using DESeq2 v1.36.0 [17]. Transcripts per million (TPM) values were calculated using StringTie v2.2.1. Differential expression analysis was performed using iDEP.96 [17], and genes with low expression (Min. CPM=4.9, n libraries=3, Pseudo count=4) were filtered out. Genes with a false discovery rate < 0.05 and |fold change| > 1.2 were identified as differentially expressed genes (DEGs). A principal component analysis plot and heatmap were generated using iDEP. Gene Ontology (GO) analysis of DEGs was performed using DAVID [25].

### Quantification of mRNA levels via quantitative PCR

Total RNA was extracted from the mouse corpus callosum or lumbar spinal cord using the *mirVana<sup>TM</sup>* miRNA Isolation Kit (Qiagen) following the manufacturer's instructions. cDNA was prepared and amplified from 500 ng of brain total RNA or 400 ng of lumbar spinal cord total RNA using the PrimeScript<sup>TM</sup> RT reagent Kit (Perfect Real Time) (TaKaRa Bio, Kusatsu, Japan). One-fiftieth of the resulting cDNA yield was amplified with TB Green Premix Ex Taq<sup>TM</sup> II (Tli RNaseH Plus) (TaKaRa

Bio) using the Thermal Cycler Dice Real Time System II (TaKaRa Bio). The thermal cycler protocol was as follows: 1 cycle at 95 °C for 30 s, 40 or 45 cycles at 95 °C for 5 s and 60 °C for 30 s, and a dissociation step at 95 °C for 15 s, 60 °C for 30 s, and 95 °C for 15 s.  $\beta$ -actin was used as an internal control.

The primers used for quantitative PCR are listed in Additional file 1: Table S1B.

### Statistical analyses

All semiquantitative immunoblotting data, behavioral tests, Woelcke staining, immunofluorescence staining, toluidine blue staining, and quantitative PCR results were analyzed using one-way analysis of variance (ANOVA) followed by multiple comparison tests with Sidak's correction for three groups and Welch's t-tests for two groups. Statistical analyses were performed using GraphPad Prism software (GraphPad Software, La Jolla, CA, USA). No randomization or blinding procedures were employed in this study.

## Results

### Generation of transgenic mice conditionally overexpressing the ALS-linked mutant TDP-43 in oligodendrocytes

To investigate the effects of excess TDP-43<sup>M337V</sup> levels in oligodendrocytes, we established a conditional transgenic mouse model expressing human TDP-43 with the ALS-linked p.M337V mutation (hTDP-43<sup>M337V</sup>-cTg) using the Cre/LoxP system (Fig. 1A). The targeting vector incorporated four stop sequences flanked by the loxP sequence to prevent leaky expression of TDP-43<sup>M337V</sup> under the CAG promoter, and it was integrated into the *Rosa26* locus via homologous recombination. We specifically chose TDP-43<sup>M337V</sup> owing to the well-characterized role of the p.M337V TARDBP gene mutation in ALS pathogenesis [57]. Previous studies from our group indicated that TDP-43<sup>M337V</sup> exhibits an extended protein half-life compared with other ALS-causative TDP-43 mutations, correlating with earlier disease onset [68], and that a TDP-43<sup>M337V</sup> knock-in mouse model showed deregulated splicing [69].

To assess the neurotoxic effects resulting from ubiquitous overexpression of hTDP-43<sup>M337V</sup>, we genetically ablated the floxed stop sequences from both alleles (CAG-hTDP-43<sup>M337V</sup>-+/+). CAG-hTDP-43<sup>M337V</sup>-+/+ mice showed stunted growth and severe clasping behaviors (Additional file 2: Movie S1; Additional file 3: Movie S2). Notably, although heterozygous CAG-hTDP-43<sup>M337V</sup>-+/wt mice survived beyond one year without observable phenotypic abnormalities, homozygous CAG-hTDP-43<sup>M337V</sup>-+/+ mice did not survive beyond 50 days (mean survival = 32.44 ± 6.2 days; Additional file 4: Fig. S2).

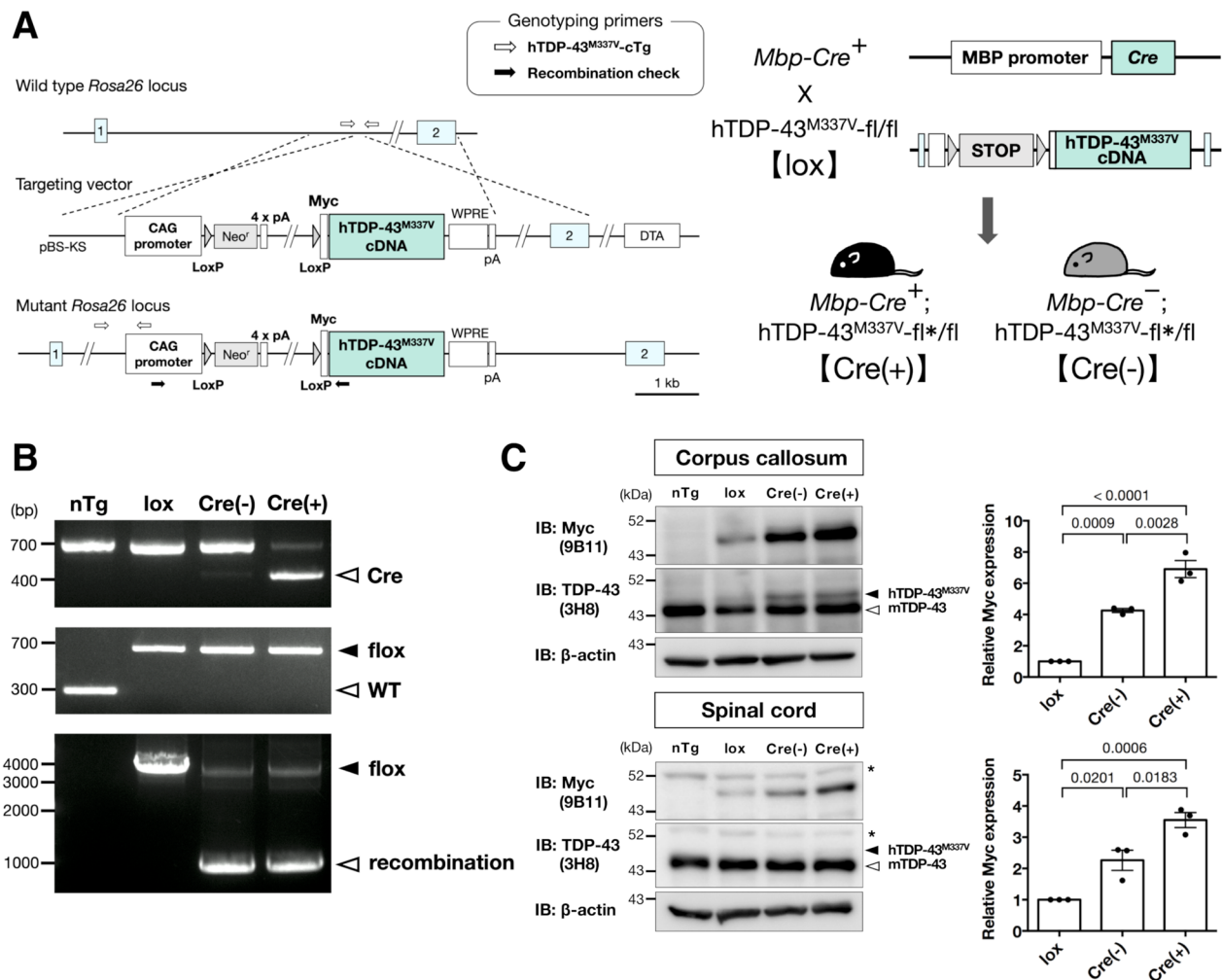


**Fig. 1** Generation and characterization of oligodendrocyte-specific human TDP-43<sup>M337V</sup> transgenic mice. **A** Left: Schematic of the murine *Rosa26* locus, the gene-targeting vector for inserting the floxed human TDP-43<sup>M337V</sup> expression cassette, and the resultant mutant *Rosa26* locus after homologous recombination. Human TDP-43<sup>M337V</sup> cDNA under the control of the CAG promoter, interrupted by a neomycin resistance gene (Neo<sup>r</sup>) and polyA sequences flanked by loxP sequences, was integrated into the *Rosa26* locus. A Myc-Tag was inserted at the N-terminal end of hTDP-43 cDNA. DTA: diphtheria toxin A fragment; WPRE: woodchuck hepatitis virus posttranscriptional regulatory element. Right: Schematic of crossbreeding to generate *Mbp-Cre*; hTDP-43<sup>M337V</sup>-fl/fl mice. Asterisks indicate recombinant alleles. **B** Representative genotyping images of nontransgenic mice (nTg), hTDP-43<sup>M337V</sup>-fl/fl mice (lox), *Mbp-Cre*<sup>-</sup>; hTDP-43<sup>M337V</sup>-fl/fl mice [Cre(-)] and *Mbp-Cre*<sup>+</sup>; hTDP-43<sup>M337V</sup>-fl/fl mice [Cre(+)] from PCR. Genotyping results of Cre recombinase (top), the mutant *Rosa26* locus carrying the floxed TDP-43<sup>M337V</sup> cassette (middle), and Cre-dependent recombination (bottom). Image showing Cre-dependent recombination also occurring in Cre(-). White and black arrows in (A) indicate specific primers for PCR of the mutant *Rosa26* locus and Cre-dependent recombination, respectively. **C** Representative immunoblotting images showing Myc-hTDP-43<sup>M337V</sup> expression. Lysates from the corpus callosum and lumbar spinal cord of mice with the specified genotype were subjected to immunoblotting using anti-Myc, anti-TDP-43, or anti-β-actin antibodies. Asterisks denote nonspecific bands. Relative myc expression levels are presented as means ± standard errors of the mean (SEMs). *P*-values were determined using one-way ANOVA followed by Tukey–Kramer multiple comparison tests (*n* = 3)

These results indicate that hTDP-43<sup>M337V</sup> exhibits dose-dependent toxicity.

Next, we established a mouse model overexpressing TDP-43<sup>M337V</sup> specifically in oligodendrocytes by crossing hTDP-43<sup>M337V</sup>-fl/fl mice with *Mbp-Cre* mice (Fig. 1A, Additional file 4: Fig. S3). *Mbp-Cre* mice harbor Cre recombinase cDNA driven by the endogenous

*Mbp* promoter. We validated the cell-type specificity of Cre-dependent recombination using *Rosa*-NLS-LacZ reporter mice, which express nuclear β-galactosidase in a Cre-dependent manner. Our analysis confirmed that most of the β-galactosidase-positive cells expressed Olig2, a transcription factor serving as an oligodendrocyte marker in the corpus callosum and the lumbar

spinal cord of *Mbp-Cre<sup>+</sup>*; *Rosa-NLS-LacZ* mice (Additional file 4: Fig. S4A). Subsequently, we crossed *Mbp-Cre<sup>+</sup>* mice with hTDP-43<sup>M337V</sup>-fl/fl mice. Considering the dose-dependent toxicity of TDP-43<sup>M337V</sup>, we analyzed mice carrying homozygous hTDP-43<sup>M337V</sup> alleles. Designed PCR primers (Fig. 1A, black arrows) were used to detect Cre-dependent recombination. During the second crossbreeding step, Cre-dependent recombination unexpectedly occurred in tail samples, regardless of the Cre transgene's presence (Fig. 1B, bottom). Nevertheless, we confirmed a Cre-dependent increase in TDP-43<sup>M337V</sup> expression in the corpus callosum and the spinal cord (Fig. 1C). Notably, we confirmed that *Mbp-Cre*-dependent recombination did not occur in motor neurons, microglia, or astrocytes in the central nervous system (Additional file 4: Fig. S4B).

From these observations, we speculated that the transient ectopic Cre expression in germ cells induced heterozygous systemic recombination. Therefore, we designated mice carrying the Cre transgenes as *Mbp-Cre<sup>+</sup>*; hTDP-43-fl\*/fl [Cre(+)] and their Cre transgene-negative littermates as *Mbp-Cre<sup>-</sup>*; hTDP-43-fl\*/fl [Cre(-)], where asterisks indicate systemic recombination. Consistent with this notion, we successfully confirmed an increase in TDP-43<sup>M337V</sup> expression in the nuclei of Cre(+) mouse oligodendrocytes (Additional file 4: Fig. S5, 6).

#### Overexpression of TDP-43<sup>M337V</sup> in oligodendrocytes exacerbates motor dysfunction in mice

To determine the consequences of TDP-43<sup>M337V</sup> overexpression in oligodendrocytes, we performed behavioral tests in wild-type C57BL/6J (nTg), Cre(-), and Cre(+) mice. Both Cre(-) and Cre(+) mice were born at the expected Mendelian ratio and developed normally. Male Cre(+) mice showed lower body weights compared with Cre(-) mice from 6 months of age, with this trend becoming more pronounced as the mice aged; however, the average body weight of female Cre(+) mice remained unaffected (Fig. 2A). Hindlimb clasping, which is indicative of motor dysfunction in various neurodegenerative disease models [53], was observed in Cre(+) mice starting at 3 months of age, with nearly 90% of these mice displaying clasping signs by 12 months of age (Fig. 2B). The balance beam test, assessing motor dysfunction, including motor coordination deficits, showed that both Cre(-) and Cre(+) mice could traverse the 24-mm-wide beam smoothly, similar to nTg mice (data not shown). When crossing the narrower 14-mm-wide beam, there were no differences in crossing times among genotypes (Fig. 2C, top left). Although both Cre(-) and Cre(+) showed a significant increase in the number of total steps (Fig. 2C, top right), we observed a Cre-dependent increase in the number of total hindpaw slips (Fig. 2C, bottom left)

as well as the number of slips normalized by the total number of steps (Fig. 2C, bottom right; Additional file 5: Movie S3; Additional file 6: Movie S4). Additional tests, including grip strength, rotarod, and stride length tests, did not reveal discernible differences between Cre(-) and Cre(+) mice (Fig. 2D, E, F).

#### TDP-43<sup>M337V</sup> overexpression in oligodendrocytes induces myelin pallor in the white matter of the brain and spinal cord

To elucidate the underlying cause of motor dysfunction, we analyzed the brains and spinal cords of 12-month-old mice. First, we investigated the effects of TDP-43<sup>M337V</sup> overexpression in oligodendrocytes. Using Woelcke staining, which stains myelin sheaths, we observed myelin pallor in the corpus callosum and white matter of the lumbar spinal cords of Cre(+) mice (Fig. 3A), suggesting damage to myelinating oligodendrocytes. However, the number of oligodendrocytes [assessed via adenomatous polyposis coli (APC)] and the number of OPCs [assessed via platelet-derived growth factor receptor  $\alpha$  (PDGFR $\alpha$ /CD140)] in the white matter of Cre(+) mice remained unaffected (Fig. 3B). Additionally, we confirmed that differentiation was not impaired in OPCs isolated from neonatal Cre(+) mice (Additional file 4: Fig. S7). Given that *Mbp-Cre* mice do not exhibit peripheral nerve recombination [40], Schwann cells expressing *Mbp* were unaffected. Accordingly, the number and integrity of axons in the ventral roots of lumbar spinal nerves (assessed via Toluidine blue staining) were also unaffected (Additional file 4: Fig. S8A). Furthermore, the number of ChAT-positive motor neurons remained unchanged, and their morphology was unaltered in the ventral horn of the lumbar spinal cord across genotypes (Additional file 4: Fig. S8B).

#### RNA-seq analysis reveals that TDP-43<sup>M337V</sup> overexpression leads to oligodendrocyte dysfunction

To elucidate the mechanisms underlying oligodendrocyte dysfunction, we performed RNA sequencing of oligodendrocyte lineage cells isolated from the whole brains of nTg or Cre(+) mice at 12 months of age using MACS (Fig. 4A). We isolated and pooled PDGFR $\alpha$ -positive OPCs and O1- and/or O4-positive oligodendrocytes to assess the population of oligodendrocyte lineage cells. The TPM values, read counts normalized by gene length [66], of representative oligodendrocyte markers [1, 18, 26, 36], i.e., *Mbp*, *Plp1*, and *Cnp*, were markedly higher than those of neuronal or other glial cell markers (Fig. 4B; Additional file 1: Table S2A), indicating that the RNA-seq samples were enriched in oligodendrocytes. Subsequently, we analyzed the raw read counts using iDEP [17]. Principal component analysis clearly distinguished the Cre(+) group from the nTg group (Fig. 4C,

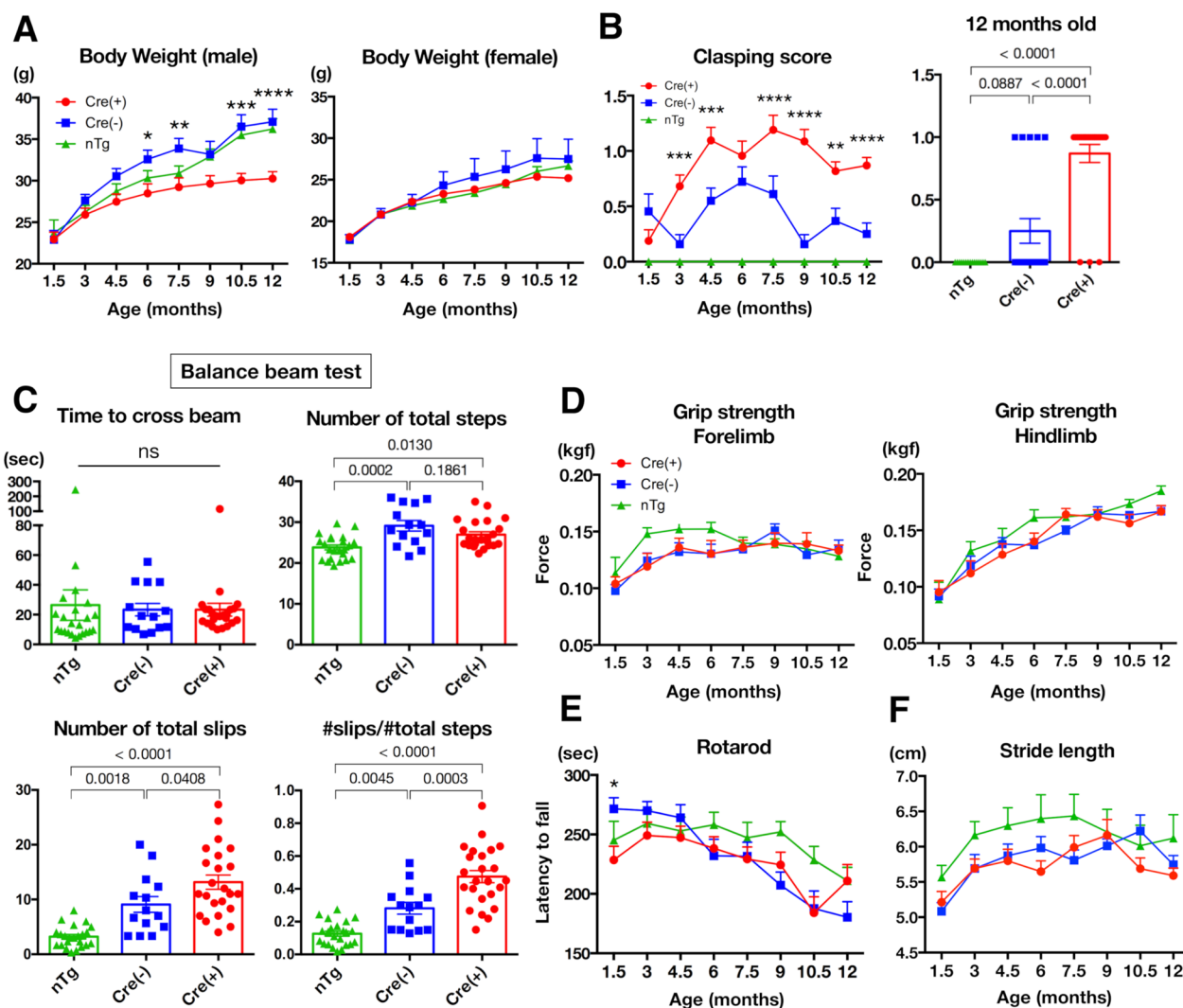


**Fig. 2** TDP-43<sup>M337V</sup> overexpression in oligodendrocytes exacerbates motor dysfunction in mice. **A** Body weights of nTg [n = 25 (male: 11; female: 14)], Cre(-) [n = 20 (male: 12; female: 8)], and Cre(+) [n = 23 (male: 10; female: 13)] mice were plotted according to age. Male Cre(+) mice exhibited lower body weights. **B** Claspings signs were scored at indicated ages on a 0 (no phenotype) to 3 (severe phenotype) scale [left: nTg: n = 16; Cre(-): n = 20; Cre(+): n = 23]. Claspings scores at 12 months are shown as a bar graph for mice with specific genotypes (right). Approximately 90% of Cre(+) mice (20/23) exhibited mild claspings signs at 12 months of age (right). **C** Results of balance beam tests using a 14-mm-wide beam. Average beam crossings, total steps, total hindpaw slips, and the slip ratio (total slips to total steps) are plotted [nTg: n = 23; Cre(-): n = 14; Cre(+): n = 23]. **D** Phenotype scoring in the grip strength test [(male nTg: n = 11; Cre(-): n = 10; Cre(+): n = 9)], **E** rotarod test [(nTg: n = 25; Cre(-): n = 20; Cre(+): n = 23)], and **F** stride length test [(male nTg: n = 8; Cre(-): n = 12; Cre(+): n = 10)]. Scores for body weight, claspings, grip strength, rotarod performance, and stride length are presented as means ± SEMs; *p*-values were determined via two-way ANOVA followed by Sidak's multiple comparisons test. Claspings scores at 12 months are presented as means ± SEMs; *p*-values were determined via one-way ANOVA followed by Tukey–Kramer multiple comparison tests. \**p* < 0.05, \*\**p* < 0.01, \*\*\**p* < 0.001, and \*\*\*\**p* < 0.0001

left). Differential gene expression analysis identified 4870 genes significantly altered in Cre(+) samples compared with nTg samples: 2342 and 2528 genes were downregulated and upregulated, respectively (Fig. 4C, right; Additional file 1: Table S2B–D). Downregulation of markers of myelinating oligodendrocytes, such as *Mbp* and *Mobp*, as well as *Sc116a1* (i.e., monocarboxylate transporter 1), involved in proper myelination [34] (Fig. 4D), suggested

impaired myelination. Moreover, genes involved in the cholesterol biosynthesis pathway, critical for myelin formation, with the myelin sheath containing 70%–80% of the cholesterol in the brain [11], were significantly downregulated (Fig. 4E), also indicating impaired myelination. GO enrichment analysis of DEGs (*q*-value < 0.05, |fold change| > 1.2; Additional file 1: Tables S2E, F) highlighted activation of immune system pathways and

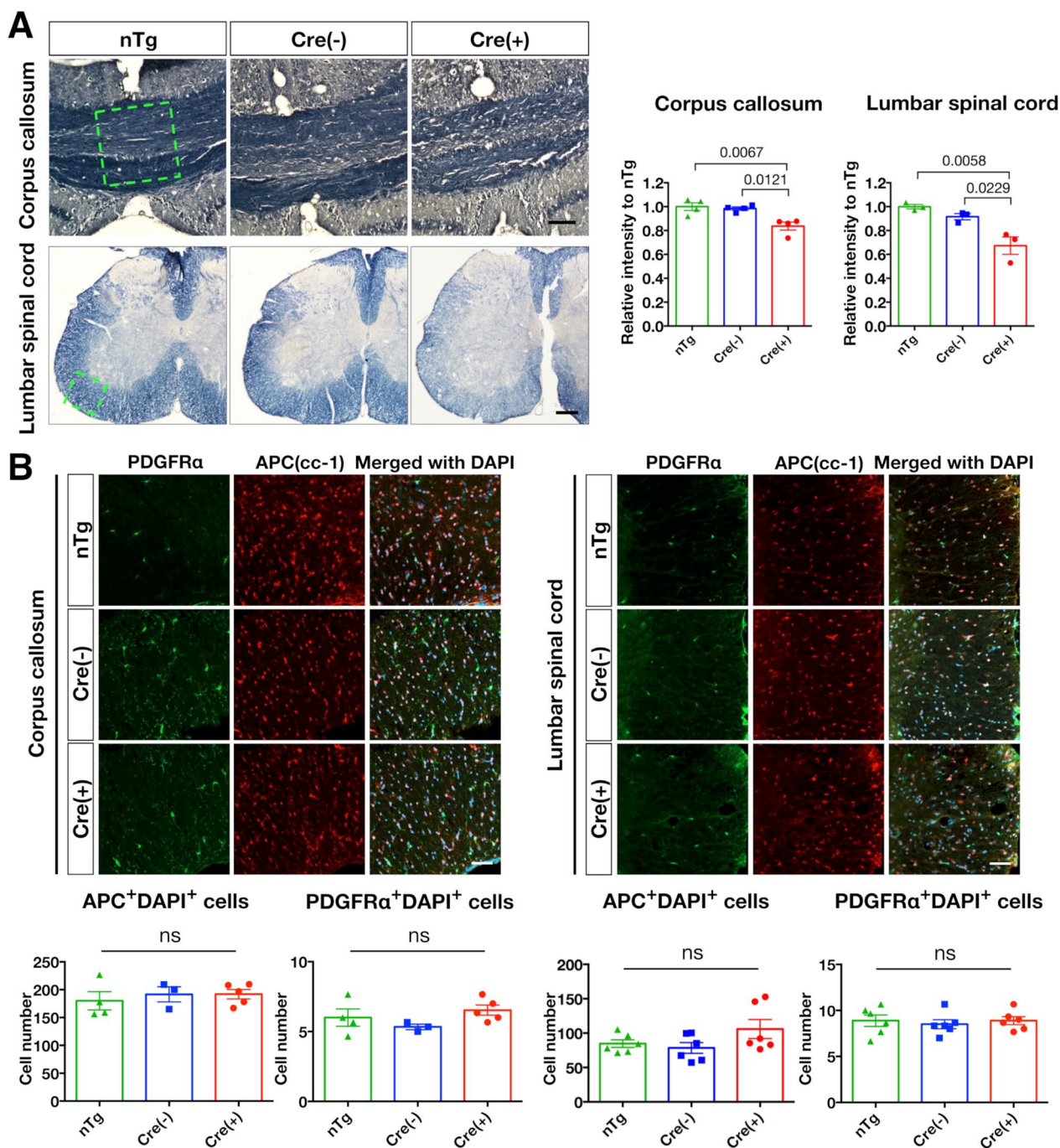


**Fig. 3** Myelin pallor observed in the white matter of *Mbp-Cre<sup>+</sup>; hTDP-43<sup>M337V-f1\*/f1</sup>* mice. **A** Representative images of Woelcke staining and quantification relative to nTg in the regions indicated by dashed squares in the corpus callosum and the white matter of the lumbar spinal cord in 12-month-old mice (n=4 sections per mouse for the corpus callosum, n=3 sections per mouse for the lumbar spinal cord). **B** Representative immunofluorescence images of OPCs (PDGFRα, green) and oligodendrocytes (APC, red) in the corpus callosum and the lumbar spinal cord of 12-month-old mice. Mean number of PDGFRα/DAPI- or APC/DAPI-double-positive cells was quantified and plotted (per 0.09 mm<sup>2</sup> of the corpus callosum, per 0.1 mm<sup>2</sup> of the white matter of the lumbar spinal cord, n=3 sections per mouse). Number of oligodendrocytes and OPCs did not differ significantly among genotypes. Data are presented as means ± SEMs. *P*-values were determined using one-way ANOVA followed by Tukey–Kramer multiple comparison tests. Scale bars: 10 μm (A, upper panel), 20 μm (A, lower panel), and 50 μm (B)

inflammatory response in Cre(+) oligodendrocyte lineage cells (Fig. 4F). Notably, upregulation of genes related to apoptosis was observed: expression levels of tumor necrosis factor receptor 1 (*Tnfrsf1a*), a principal death receptor, and some caspases, indispensable for apoptosis induction [15], were markedly elevated in Cre(+) oligodendrocyte lineage cells (Fig. 4G). We also confirmed the Cre-dependent changes in *Mbp*, *Ng2*, *Olig2*, *Srebf2*, and *Hmgcr* mRNA expression in oligodendrocyte lineage cells isolated from whole brains of 12-month-old mice (Additional file 4: Fig. S9A). Moreover, we found Cre-dependent splicing changes in the *Sort1* and *Mbp* genes (Additional file 4: Fig. S9B, C). Both increased inclusion of exon 17b in the *Sort1* gene and an increased level of *Golli-Mbp*, a splicing form of the *Mbp* gene, are associated with increased TDP-43 function [69, 70], supporting a gain-of-toxicity mechanism of mutant TDP-43 in our model. On the other hand, neither downregulation of these myelination-related genes nor myelin pallor in the white matter was found in the 1-month-old brain of Cre(+) mice (Additional file 4: Fig. S10A, B), suggesting that Cre-dependent mutant TDP-43 expression accompanying oligodendrocyte maturation is essential for oligodendrocyte abnormalities in our model.

#### Overexpression of TDP-43<sup>M337V</sup> induces apoptosis in oligodendrocytes

Based on RNA-seq data, we examined apoptosis induction in oligodendrocytes due to TDP-43<sup>M337V</sup> overexpression. Immunostaining revealed cleaved caspase-3 in oligodendrocytes within the white matter of the brain and the lumbar spinal cord of Cre(+) mice (Fig. 5A; Additional file 4: Fig. S11). Approximately half of the cleaved caspase-3-positive oligodendrocytes colocalized with the microglial marker galectin-3 (formerly known as Mac2 antigen) (Fig. 5B; Additional file 4: S12A) or ionized calcium-binding adapter molecule 1 (Iba1) (Additional file 4: Fig. S12B) in the lumbar spinal cord, suggesting that activated microglia engulfed apoptotic oligodendrocytes.

Immunoreactivity for the microglial marker Iba1 and the astrocytic marker glial fibrillary acidic protein (GFAP) was increased in the white matter of the brain (Fig. 5C, D), suggesting gliosis. In the lumbar spinal cord, microgliosis was observed in both the gray and white matter but was more prominently in the white matter (Fig. 5C; Additional file 4: Fig. S13). Quantitative PCR confirmed microglial and astrocytic activation (Fig. 5E). Notably, despite low-level ubiquitous TDP-43<sup>M337V</sup> expression in Cre(-) mice caused by systemic recombination, oligodendrocyte apoptosis and gliosis were specific to Cre(+) mice. Consistent with the RNA-seq analysis results, *Tnf* mRNA upregulation was observed in the lumbar spinal cord of Cre(+) mice (Fig. 5E). Collectively, these findings suggest that oligodendrocytes overexpressing TDP-43<sup>M337V</sup> undergo apoptosis, triggering gliosis in microglia and astrocytes.

#### Discussion

In this study, we aimed to investigate the impact of excessive ALS-linked mutant TDP-43 expression on oligodendrocyte pathology in mice. To achieve this, we established a novel mouse model overexpressing human TDP-43<sup>M337V</sup> in oligodendrocytes, which exhibited motor dysfunction accompanied by oligodendrocyte apoptosis and gliosis in the white matter of the brain and lumbar spinal cord. Notably, overexpression of mutant TDP-43 damaged oligodendrocytes, particularly affecting myelination.

Our mouse model partially recapitulated ALS pathology by overexpressing ALS-linked mutant TDP-43 in oligodendrocytes. Previous studies have shown that overexpression of wild-type or ALS-linked mutant TDP-43 can induce neuronal toxicity [3, 27, 71], and even nuclear overexpression of mutant TDP-43 without cytoplasmic aggregation results in neuronal loss [3, 6, 58]. On the other hand, loss of TDP-43 in oligodendrocytes disrupts oligodendrocyte maturation [67], underscoring an essential role of TDP-43 in oligodendrocyte maintenance

(See figure on next page.)

**Fig. 4** Cholesterol biosynthetic and apoptotic pathway are deregulated in oligodendrocytes from *Mbp-Cre<sup>+</sup>; hTDP-43<sup>M337V</sup>-fl<sup>\*/fl</sup>* mice. **A** Schematic of RNA-seq analysis for oligodendrocyte lineage cells, which were isolated from the whole brains of nTg or Cre(+) mice via magnetic-activated cell sorting [nTg: n=3, Cre(+): n=3]. **B** Transcripts per million (TPM) of nTg in RNA-seq for representative markers of oligodendrocytes, microglia, astrocytes, pericytes, and neurons. Oligodendrocytes were highly enriched in the analyzed RNA-seq samples. TPM values are plotted as means ± SEMs. **C** Principal component analysis plot and heatmap of differentially expressed genes (DEGs; *q*-value < 0.05 and |fold change| > 1.2). **D** List of representative genes for oligodendrocyte lineage cell markers. Downregulated and upregulated DEGs (*q*-value < 0.05 and |fold change| > 1.2) are highlighted in blue and red, respectively. Expression levels of myelinating oligodendrocyte markers and monocarboxylate transporter 1 (*Mct1*) were downregulated in Cre(+) oligodendrocytes. **E** List of representative genes involved in cholesterol biosynthesis. *Srebf2*, the master regulator of cholesterol biosynthesis, and its downstream genes were downregulated in Cre(+) oligodendrocytes. **F** Top 10 Gene Ontology (GO) terms for biological process. GO analysis revealed the upregulation of genes related to immunity, inflammation, and apoptosis. **G** List of representative genes of apoptosis pathway-related genes. Expression levels of *Tnfrsf1a* and its downstream genes were upregulated in Cre(+). Gene IDs are presented with fold changes [Cre(+) / nTg] and *q*-values (**D**, **E**, and **G**)

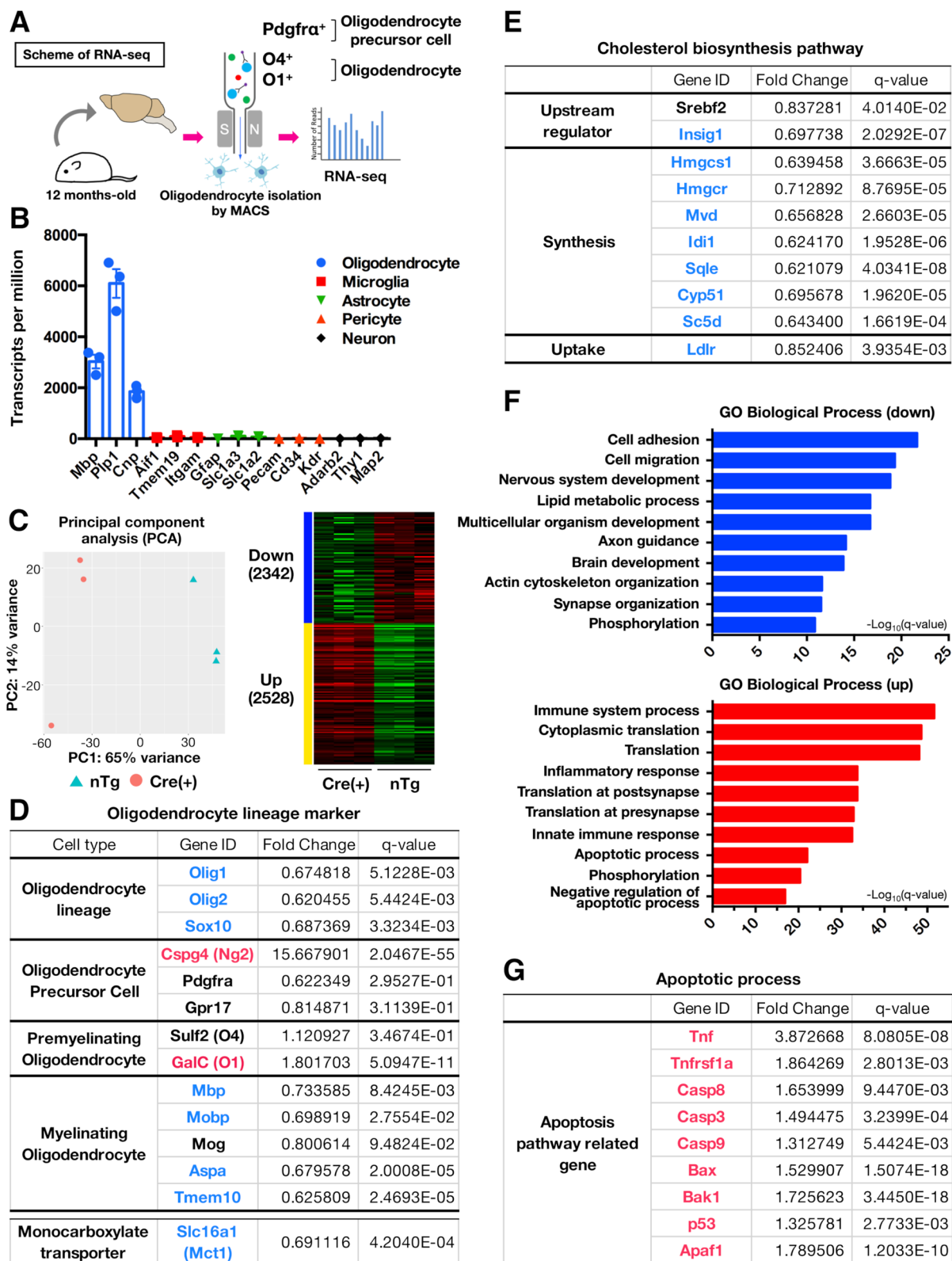


Fig. 4 (See legend on previous page.)

(Additional file 4: Fig. S1). Our study provides novel evidence that oligodendrocytes are susceptible to nuclear TDP-43 overexpression. Our findings, coupled with those of Wang et al. [67], indicate that both TDP-43 loss-of-function and gain-of-toxicity impair oligodendrocytes, similar to neurons. However, unlike typical TDP-43 pathology, characterized by cytoplasmic mislocalization and aggregation [10, 50], our mouse model did not replicate these features, consistent with most TDP-43-overexpressing rodent models. Consequently, the potential toxicity associated with cytoplasmic accumulation of TDP-43 in oligodendrocytes remains undetermined in our study. Prior studies have shown that TDP-43 monomerization is essential for facilitating cytoplasmic mislocalization and subsequent aggregation of TDP-43 [43, 46], a finding that may be key to designing the animal models that recapitulate the cytoplasmic pathology of TDP-43 in oligodendrocytes.

Although our mouse model showed Cre-dependent deterioration in motor function, including clasping behavior and increased hindpaw slips in the balance beam test, Cre(-) mice also exhibited mild motor deficits compared with nontransgenic mice. The impaired motor function observed in Cre(-) mice likely originated from recombination-mediated hemizygous systemic expression of TDP-43<sup>M337V</sup>, an unintended consequence of two-step crossbreeding involving *Mbp-Cre* and hTDP-43<sup>M337V</sup>-cTg mice, and Cre-dependent TDP-43 expression exacerbated the motor deficits. In addition, since there is a possibility that a mixed background introduced by *Mbp-Cre* mice may have caused phenotypic variation, we used littermates resulting from this crossbreeding to minimize variability in the genetic background. Despite this systemic expression of TDP-43<sup>M337V</sup> in Cre(-) mice, glial activation and cytokine upregulation were specific to Cre(+) mice. This suggests that TDP-43<sup>M337V</sup> expression levels are not sufficient to induce oligodendrocyte dysfunction in Cre(-) mice, supported by our findings that TDP-43<sup>M337V</sup> levels critically affect mouse survival (Additional file 4: Fig. S2) and previous observations that increased human wild-type or mutant TDP-43

expression levels markedly reduce mouse survival times [63, 72]. Thus, TDP-43 expression levels appear critical in its gain-of-toxicity mechanism. Additionally, our previous research revealed that the mutant TDP-43 protein half-life is inversely correlated with ALS onset, with TDP-43<sup>M337V</sup> exhibiting a longer half-life compared to other mutants [68]. This is consistent with the report of higher TDP-43 protein levels in induced pluripotent stem (iPS) cell-derived neurons from a patient with ALS carrying TDP-43<sup>M337V</sup> [4]. Taken together, these findings suggest that TDP-43<sup>M337V</sup>, with its prolonged protein half-life, represents a suitable model for studying the gain-of-toxicity mechanism associated with mutant TDP-43. In agreement with these insights, our study shows that overexpression of TDP-43<sup>M337V</sup> causes oligodendrocyte dysfunction in mice. Our study was unable to conclude whether oligodendrocyte dysfunction induced by TDP-43 overexpression alone causes motor dysfunction, i.e., whether systemic low-level TDP-43<sup>M337V</sup> expression is required to induce motor dysfunction in our model. However, we have shown that excess TDP-43 in oligodendrocytes was capable of inducing oligodendrocyte dysfunction and apoptosis with deterioration of motor function, suggesting that TDP-43-mediated oligodendrocyte dysfunction may contribute to the motor deficits characteristic of ALS. Future investigations are warranted to elucidate the gain-of-toxicity mechanism mediated by mutant TDP-43 in oligodendrocytes.

Myelin pallor and oligodendrocyte apoptosis occurred in the white matter of Cre(+) mice; however, the number of oligodendrocytes remained unaffected. RNA-seq analysis revealed downregulation of myelination- and cholesterol-related genes involved in the oligodendrocyte lineage cells of Cre(+) mice, suggesting that the remaining mutant TDP-43-overexpressing oligodendrocytes may have lost their myelination capability. Previous studies have highlighted the role of TDP-43 in cholesterol-related gene expression, particularly *SREBF2*, which encodes sterol regulatory element binding protein 2 (SREBP2), a master regulator of cholesterol homeostasis. TDP-43 binds to *SREBF2* mRNA, and TDP-43 silencing

(See figure on next page.)

**Fig. 5** Apoptosis is induced in the oligodendrocytes of the white matter from *Mbp-Cre*<sup>+</sup>; hTDP-43<sup>M337V</sup>-fl<sup>\*/fl</sup> mice. **A** Representative immunofluorescence images of lumbar spinal cords from 12-month-old mice stained for APC, cleaved caspase-3 (Cc-3), and Mac2. Bottom panels show magnified images of the areas indicated by dashed squares. Some mature oligodendrocytes expressed Cc-3. Arrowheads indicate colocalization of apoptotic oligodendrocytes and activated microglia; arrows indicate apoptotic oligodendrocytes without microglial colocalization. **B** Mean number of APC<sup>+</sup>Cc-3<sup>+</sup>Mac2<sup>+</sup> and APC<sup>+</sup>Cc-3<sup>+</sup>Mac2<sup>-</sup> cells per 0.1 mm<sup>2</sup> was quantified and plotted (n = 4 sections per mouse). **C** Representative images of the corpus callosum and white matter of the lumbar spinal cord of 12-month-old mice immunostained for Myc, Iba1, and GFAP. **D** Quantification of relative intensity to nTg per 0.1 mm<sup>2</sup> in the corpus callosum and the white matter of the lumbar spinal cord in 12-month-old mice (n = 4 sections per mouse). **E** mRNA levels of representative microglia and astrocyte markers in 12-month-old mice were determined via quantitative PCR. Data are presented as means ± SEMs; p-values were determined using one-way ANOVA followed by Tukey–Kramer multiple comparison tests. Scale bars: 50 μm (A, top), 25 μm (A, bottom), and 100 μm (C)

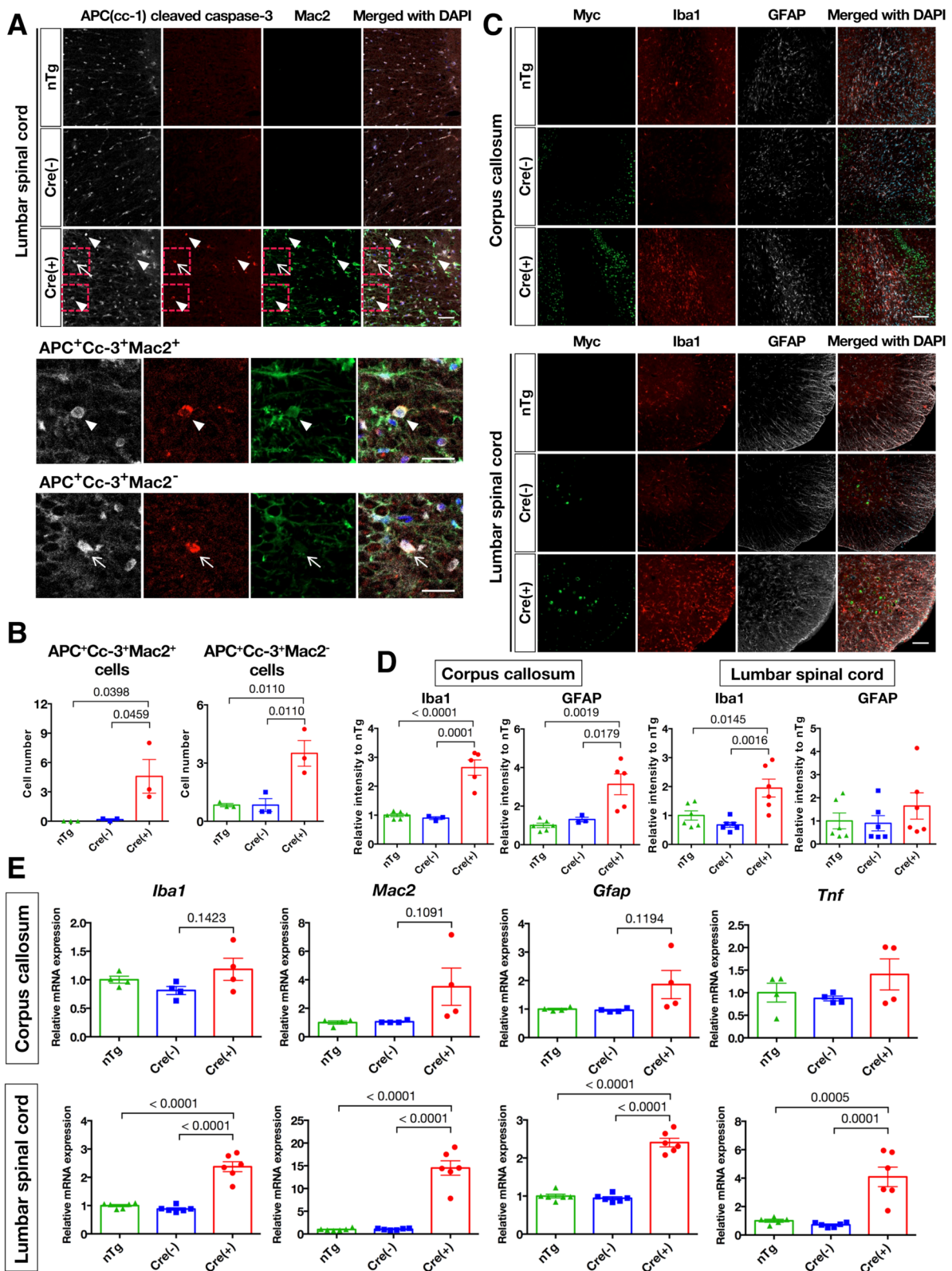


**Fig. 5** (See legend on previous page.)

reduces cleaved N-terminal SREBP2 levels in human iPS-derived oligodendrocytes [23]. In contrast, TDP-43 overexpression in human kidney cells leads to SREBP2 downregulation [14]. Collectively, these findings suggest that both TDP-43 overexpression and depletion result in SREBP2 downregulation. We provide the first evidence that TDP-43 overexpression downregulates *Srebf2* in mouse oligodendrocytes. Given that SREBP2-mediated cholesterol supply is crucial for myelination, targeting SREBP2 may mitigate TDP-43 toxicity in ALS.

In our study, excess mutant TDP-43 induced oligodendrocyte apoptosis associated with white matter gliosis. Conversely, selective deletion of TDP-43 in oligodendrocytes induces oligodendrocyte necroptosis [67]. Thus, strict regulation of TDP-43 expression is essential for the survival of oligodendrocytes. Oligodendrocyte degeneration is involved in various neurodegenerative diseases [21, 33, 48], and oligodendrocyte apoptosis is evident in ALS mouse models [30, 48]. On the other hand, in multiple system atrophy (MSA), a neurodegenerative disease characterized by misfolded  $\alpha$ -synuclein protein accumulation in neurons and oligodendrocytes [13], oligodendrocyte-specific overexpression of human  $\alpha$ -synuclein leads to  $\alpha$ -synuclein aggregates in oligodendrocytes, neuronal loss, and motor impairment in mice [73]. Thus, oligodendrocyte degeneration can cause non-cell-autonomous neurodegeneration in MSA mouse models. Conversely, our Cre(+) mice exhibited oligodendrocyte apoptosis without observable neurodegeneration, suggesting distinct toxicity mechanisms between TDP-43 and  $\alpha$ -synuclein. Propagation of  $\alpha$ -synuclein pathology is a key feature in  $\alpha$ -synuclein-mediated neurodegeneration [51]. However, TDP-43 aggregates exhibit a lower propagation than expected [62], and differences in propagation activity may influence non-cell-autonomous neurodegeneration in each model. Further studies are required to determine the role of TDP-43 in non-cell-autonomous neurodegeneration, especially through oligodendrocytes in ALS.

Microgliosis and astrogliosis were predominant in the white matter of Cre(+) mice, likely due to higher *Mbp* expression levels in white matter oligodendrocytes [29, 55]. This observation aligns with previous findings showing that Cre-dependent recombination mainly affects white matter oligodendrocytes in *Mbp-Cre* mice [40]. Myelin debris or cytokines released from damaged oligodendrocytes are known to trigger the activation of microglia and astrocytes [7, 42, 44, 45]. Our results suggest that oligodendrocyte dysfunction triggers neuroinflammation and that reactive glial cells further exacerbate inflammation of oligodendrocytes in Cre(+) mice. Although our study suggests that mutant TDP-43 induces oligodendrocyte apoptosis mainly via cell-autonomous mechanism, surrounding neuroinflammatory response may also

contribute to oligodendrocyte apoptosis in a non-cell-autonomous manner. Further investigation of the cross-talk between oligodendrocytes and surrounding reactive glial cells in our mouse model will provide the complete picture of oligodendrocyte dysfunction in ALS.

## Conclusions

We established a mouse model overexpressing the ALS-linked mutant TDP-43 in oligodendrocytes, with model mice showing mild motor dysfunction, myelin pallor, and gliosis. RNA-seq revealed downregulation of myelin-related genes and upregulation of apoptosis-related genes in the oligodendrocyte lineage cells of transgenic mice. Oligodendrocyte apoptosis associated with microgliosis/astrogliosis predominated in the white matter of mice, potentially exacerbating neuroinflammation. Overall, our study identified oligodendrocytes as potential therapeutic targets for ALS.

## Abbreviations

APC-cc1	Adenomatous polyposis coli, clone cc-1
ALS	Amyotrophic lateral sclerosis
Cc-3	Cleaved caspase-3
ChAT	Choline acetyltransferase
DEG	Differentially expressed gene
fALS	Familial amyotrophic lateral sclerosis
FTLD	Frontotemporal lobar degeneration
GFAP	Glial fibrillary acidic protein
GO	Gene ontology
HMGCR	3-Hydroxy-3-methylglutaryl coenzyme A reductase
Iba1	Ionized calcium-binding adapter molecule 1
MACS	Magnetic-activated cell sorting
Mbp	Myelin basic protein
Mct1	Monocarboxylate transporter 1
PDGFR $\alpha$	Platelet-derived growth factor receptor $\alpha$
NLS	Nuclear localization signal
nTg	Nontransgenic
OPC	Oligodendrocyte precursor cell
sALS	Sporadic amyotrophic lateral sclerosis
SREBF2	Sterol regulatory element-binding factor 2
SOD1	Cu/Zn superoxide dismutase
TDP-43	TAR DNA-binding protein 43
TPM	Transcripts per million
WPRE	Woodchuck hepatitis virus posttranscriptional regulatory element

## Supplementary Information

The online version contains supplementary material available at <https://doi.org/10.1186/s40478-024-01893-x>.

Additional file 1: **Table S1.** Lists of primers. **Table S1A.** A list of genotyping PCR primers. **Table S1B.** A list of quantitative PCR primers. **Table S2.** Assembled multiple supplementary tables containing data for RNA sequencing. **Table S2A.** Transcripts per million. **Table S2B.** Genes expressed in oligodendrocyte lineage cells of 12-month-old *Mbp-Cre*<sup>+</sup>; hTDP-43<sup>M337V</sup>-fl\*/fl mice. **Table S2C.** Genes downregulated ( $q$ -value < 0.05 and fold change < -1.2) in oligodendrocyte lineage cells of 12-month-old *Mbp-Cre*<sup>+</sup>; hTDP-43<sup>M337V</sup>-fl\*/fl mice. **Table S2D.** Genes upregulated ( $q$ -value < 0.05 and fold change > 1.2) in oligodendrocyte lineage cells of 12-month-old *Mbp-Cre*<sup>+</sup>; hTDP-43<sup>M337V</sup>-fl\*/fl mice. **Table S2E.** Gene ontology terms downregulated in oligodendrocyte lineage cells of 12-month-old *Mbp-Cre*<sup>+</sup>; hTDP-43<sup>M337V</sup>-fl\*/fl mice. **Table S2F.** Gene ontology terms

upregulated in oligodendrocyte lineage cells of 12-month-old *Mbp-Cre<sup>+</sup>*; hTDP-43<sup>M337V</sup>-fl\*/fl mice.

Additional file 2: **Movie S1.** Hindlimb paralysis of a homozygous CAG-hTDP-43<sup>M337V</sup>-+/+ mouse

Additional file 3: **Movie S2.** Hindlimb clasping of a homozygous CAG-hTDP-43<sup>M337V</sup>-+/+ mouse

Additional file 4: **Figure S1.** Summary of TDP-43-based rodent models focusing on motor neurons or oligodendrocytes **Figure S2.** Ubiquitous overexpression of TDP-43<sup>M337V</sup> causes early lethality in mice. **Figure S3.** Schematic of crossbreeding to generate *Mbp-Cre*; hTDP-43<sup>M337V</sup>-fl\*/fl mice **Figure S4.** Cre-dependent recombination occurs in the oligodendrocytes of *Mbp-Cre<sup>+</sup>*; *Rosa-NLS-LacZ-fl/wt* mice. **Figure S5.** Oligodendrocytes overexpress TDP-43<sup>M337V</sup> in *Mbp-Cre<sup>+</sup>*; hTDP-43<sup>M337V</sup>-fl\*/fl mice. **Figure S6.** Endogenous TDP-43 localizes in the nucleus of *Mbp-Cre<sup>+</sup>*; hTDP-43<sup>M337V</sup>-fl\*/fl mice overexpressing TDP-43<sup>M337V</sup>. **Figure S7.** Differentiation is not impaired in oligodendrocyte precursor cells of *Mbp-Cre<sup>+</sup>*; hTDP-43<sup>M337V</sup>-fl\*/fl mice. **Figure S8.** Motor neuronal loss in the lumbar spinal cord is not observed in *Mbp-Cre<sup>+</sup>*; hTDP-43<sup>M337V</sup>-fl\*/fl mice. **Figure S9.** The genes involved in myelination are downregulated in oligodendrocyte lineage cells of *Mbp-Cre<sup>+</sup>*; hTDP-43<sup>M337V</sup>-fl\*/fl mice. **Figure S10.** Oligodendrocyte dysfunction is not observed in *Mbp-Cre<sup>+</sup>*; hTDP-43<sup>M337V</sup>-fl\*/fl mice at 1 month of age. **Figure S11.** Activation of caspase-3 with gliosis in the corpus callosum and the cerebellum of *Mbp-Cre<sup>+</sup>*; hTDP-43<sup>M337V</sup>-fl\*/fl mice **Figure S12.** Activated microglia engulf oligodendrocytes in the white matter of *Mbp-Cre<sup>+</sup>*; hTDP-43<sup>M337V</sup>-fl\*/fl mice. **Figure S13.** Gliosis in the white matter of the lumbar spinal cord from *Mbp-Cre<sup>+</sup>*; hTDP-43<sup>M337V</sup>-fl\*/fl mice.

Additional file 5: **Movie S3.** The balance beam test of a *Mbp-Cre<sup>-</sup>*; hTDP-43<sup>M337V</sup>-fl\*/fl mice

Additional file 6: **Movie S4.** The balance beam test of a *Mbp-Cre<sup>+</sup>*; hTDP-43<sup>M337V</sup>-fl\*/fl mice

#### Acknowledgements

We thank Center for Animal Research and Education (CARE), Nagoya University for technical support on animal experiments.

#### Author contributions

MH, SW, and KY designed the study. MH and SW performed the experiments with support from OK under the supervision of KY. MS, and TO performed next generation sequence data analysis. ET and KK established the hTDP43<sup>M337V</sup>-cTg mice, and SI provided the RNZ mice and a critical input for a design of hTDP-43<sup>M337V</sup>-cTg mice. MH, SW, and KY interpreted the data, and wrote the manuscript. All the authors approved the manuscript. MH and SW are equally contributed to this work.

#### Funding

This work was supported by Grants-in-Aid for Scientific Research JP17H04986 and JP23K06826 (SW), JP19KK0214 and JP22H00467 (KY) from the Ministry of Education, Culture, Sports, Science and Technology (MEXT), Japan / Japan Society for the Promotion of Science (JSPS); AMED under Grant Numbers JP22ek0109426, JP24wm0425014, and JP24wm0625301 (KY); Uehara Memorial Foundation (to SW). MH was supported by a scholarship from Takeda Science Foundation.

#### Availability of data and materials

Data, material and software information supporting the conclusions of this article is included within the article and its additional files. The raw RNA-seq datasets analyzed in the current study are available from the corresponding author on reasonable request, and will be deposited to a public data repository.

#### Declarations

##### Ethics approval and consent to participate

The experiments using genetically modified mice were approved by the Animal Care and Use Committee and the recombinant DNA experiment

committee of Nagoya University (approval numbers RIEM240005, and #143, respectively).

##### Consent for publication

Not applicable.

##### Competing interests

The authors report no biomedical financial interests or potential conflicts of interest.

##### Author details

<sup>1</sup>Department of Neuroscience and Pathobiology, Research Institute of Environmental Medicine, Nagoya University, Chikusa-Ku, Nagoya, Aichi 464-8601, Japan. <sup>2</sup>Department of Neuroscience and Pathobiology, Graduate School of Medicine, Nagoya University, Nagoya, Aichi 466-8550, Japan. <sup>3</sup>Department of Biomedicine, Graduate School of Medical Sciences, Kyushu University, Fukuoka 812-8582, Japan. <sup>4</sup>Support Unit for Bio-Material Analysis, Research Resources Division, RIKEN Center for Brain Science, Saitama 351-0198, Japan. <sup>5</sup>Laboratory of Behavioral Genetics, RIKEN Center for Brain Science, Saitama 351-0198, Japan. <sup>6</sup>Department of Genetics, Research Institute of Environmental Medicine, Nagoya University, Aichi 464-8601, Japan. <sup>7</sup>Department of Human Genetics and Molecular Biology, Nagoya University Graduate School of Medicine, Aichi 466-8550, Japan. <sup>8</sup>Institute for Glyco-Core Research (iGCORE), Nagoya University, Aichi, Japan. <sup>9</sup>Center for One Medicine Innovative Translational Research (COMIT), Nagoya University, Aichi, Japan. <sup>10</sup>Research Institute for Quantum and Chemical Innovation, Institutes of Innovation for Future Society, Nagoya University, Aichi, Japan.

Received: 1 July 2024 Accepted: 17 November 2024

Published online: 27 November 2024

#### References

1. Akay LA, Effenberger AH, Tsai LH (2021) Cell of all trades: oligodendrocyte precursor cells in synaptic, vascular, and immune function. *Genes Dev* 35:180–198. <https://doi.org/10.1101/gad.344218.120>
2. Arai T, Hasegawa M, Akiyama H, Ikeda K, Nonaka T, Mori H, Mann D, Tsuchiya K, Yoshida M, Hashizume Y et al (2006) TDP-43 is a component of ubiquitin-positive tau-negative inclusions in frontotemporal lobar degeneration and amyotrophic lateral sclerosis. *Biochem Biophys Res Commun* 351:602–611. <https://doi.org/10.1016/j.bbrc.2006.10.093>
3. Arnold ES, Ling SC, Huelga SC, Lagier-Tourenne C, Polymenidou M, Ditsworth D, Kordasiewicz HB, McAlonis-Downes M, Platoshyn O, Parone PA et al (2013) ALS-linked TDP-43 mutations produce aberrant RNA splicing and adult-onset motor neuron disease without aggregation or loss of nuclear TDP-43. *Proc Natl Acad Sci USA* 110:E736–745. <https://doi.org/10.1073/pnas.1222809110>
4. Bilican B, Serio A, Barmada SJ, Nishimura AL, Sullivan GJ, Carrasco M, Phatnani HP, Puddifoot CA, Story D, Fletcher J et al (2012) Mutant induced pluripotent stem cell lines recapitulate aspects of TDP-43 proteinopathies and reveal cell-specific vulnerability. *Proc Natl Acad Sci USA* 109:5803–5808. <https://doi.org/10.1073/pnas.1202922109>
5. Bretschneider J, Arai K, Del Tredici K, Toledo JB, Robinson JL, Lee EB, Kuwabara S, Shibuya K, Irwin DJ, Fang L et al (2014) TDP-43 pathology and neuronal loss in amyotrophic lateral sclerosis spinal cord. *Acta Neuropathol* 128:423–437. <https://doi.org/10.1007/s00401-014-1299-6>
6. Carmen-Orozco RP, Tsao W, Ye Y, Sinha IR, Chang K, Trinh VT, Chung W, Bowden K, Troncoso JC, Blackshaw S et al (2024) Elevated nuclear TDP-43 induces constitutive exon skipping. *Mol Neurodegener* 19:45. <https://doi.org/10.1186/s13024-024-00732-w>
7. Chen JF, Wang F, Huang NX, Xiao L, Mei F (2022) Oligodendrocytes and myelin: active players in neurodegenerative brains? *Dev Neurobiol* 82:160–174. <https://doi.org/10.1002/dneu.22867>
8. Chen S (2023) Ultrafast one-pass FASTQ data preprocessing, quality control, and deduplication using fastp. *iMeta*. <https://doi.org/10.1002/imt.2.107>
9. Chen S, Zhou Y, Chen Y, Gu J (2018) fastp: an ultra-fast all-in-one FASTQ preprocessor. *Bioinformatics* 34:i884–i890. <https://doi.org/10.1093/bioinformatics/bty560>

10. de Boer EMJ, Orié VK, Williams T, Baker MR, De Oliveira HM, Polvikoski T, Silsby M, Menon P, van den Bos M, Halliday GM et al (2020) TDP-43 proteinopathies: a new wave of neurodegenerative diseases. *J Neurol Neurosurg Psychiatry* 92:86–95. <https://doi.org/10.1136/jnnp-2020-322983>
11. Dietschy JM, Turley SD (2004) Thematic review series: brain Lipids. Cholesterol metabolism in the central nervous system during early development and in the mature animal. *J Lipid Res* 45:1375–1397. <https://doi.org/10.1194/jlr.R400004-JLR200>
12. Donde A, Sun M, Ling JP, Braunstein KE, Pang B, Wen X, Cheng X, Chen L, Wong PC (2019) Splicing repression is a major function of TDP-43 in motor neurons. *Acta Neuropathol* 138:813–826. <https://doi.org/10.1007/s00401-019-02042-8>
13. Duda JE, Lee VM, Trojanowski JQ (2000) Neuropathology of synuclein aggregates. *J Neurosci Res* 61:121–127. [https://doi.org/10.1002/1097-4547\(20000715\)61:2%3c121::AID-JNRI%3e3.0.CO;2-4](https://doi.org/10.1002/1097-4547(20000715)61:2%3c121::AID-JNRI%3e3.0.CO;2-4)
14. Egawa N, Izumi Y, Suzuki H, Tsuge I, Fujita K, Shimano H, Izumikawa K, Takahashi N, Tsukita K, Enami T et al (2022) TDP-43 regulates cholesterol biosynthesis by inhibiting sterol regulatory element-binding protein 2. *Sci Rep* 12:7988. <https://doi.org/10.1038/s41598-022-12133-4>
15. Elmore S (2007) Apoptosis: a review of programmed cell death. *Toxicol Pathol* 35:495–516. <https://doi.org/10.1080/01926230701320337>
16. Ferraiuolo L, Meyer K, Sherwood TW, Vick J, Likhite S, Frakes A, Miranda CJ, Braun L, Heath PR, Pineda R et al (2016) Oligodendrocytes contribute to motor neuron death in ALS via SOD1-dependent mechanism. *Proc Natl Acad Sci USA* 113:E6496–E6505. <https://doi.org/10.1073/pnas.1607496113>
17. Ge SX, Son EW, Yao R (2018) iDEP: an integrated web application for differential expression and pathway analysis of RNA-Seq data. *BMC Bioinf* 19:534. <https://doi.org/10.1186/s12859-018-2486-6>
18. Goldman SA, Kuypers NJ (2015) How to make an oligodendrocyte. *Development* 142:3983–3995. <https://doi.org/10.1242/dev.126409>
19. Goutman SA, Hardiman O, Al-Chalabi A, Chio A, Savelieff MG, Kiernan MC, Feldman EL (2022) Emerging insights into the complex genetics and pathophysiology of amyotrophic lateral sclerosis. *Lancet Neurol* 21:465–479. [https://doi.org/10.1016/S1474-4422\(21\)00414-2](https://doi.org/10.1016/S1474-4422(21)00414-2)
20. Guyenet SJ, Furrer SA, Damian VM, Baughan TD, La Spada AR, Garden GA (2010) A simple composite phenotype scoring system for evaluating mouse models of cerebellar ataxia. *J Vis Exp*. <https://doi.org/10.3791/1787>
21. Han S, Gim Y, Jang EH, Hur EM (2022) Functions and dysfunctions of oligodendrocytes in neurodegenerative diseases. *Front Cell Neurosci* 16:1083159. <https://doi.org/10.3389/fncel.2022.1083159>
22. Heo D, Ling JP, Molina-Castro GC, Langseth AJ, Waisman A, Nave KA, Möbius W, Wong PC, Bergles DE (2022) Stage-specific control of oligodendrocyte survival and morphogenesis by TDP-43. *Elife*. <https://doi.org/10.7554/eLife.75230>
23. Ho WY, Chang JC, Lim K, Cazenave-Gassiot A, Nguyen AT, Foo JC, Muralidharan S, Viera-Ortiz A, Ong SJM, Hor JH et al (2021) TDP-43 mediates SREBF2-regulated gene expression required for oligodendrocyte myelination. *J Cell Biol*. <https://doi.org/10.1083/jcb.201910213>
24. Huang C, Tong J, Bi F, Zhou H, Xia XG (2012) Mutant TDP-43 in motor neurons promotes the onset and progression of ALS in rats. *J Clin Invest* 122:107–118. <https://doi.org/10.1172/JCI59130>
25. Huang DW, Sherman BT, Lempicki RA (2009) Systematic and integrative analysis of large gene lists using DAVID bioinformatics resources. *Nat Protoc* 4:44–57. <https://doi.org/10.1038/nprot.2008.211>
26. Huang H, He W, Tang T, Qiu M (2023) Immunological markers for central nervous system Glia. *Neurosci Bull* 39:379–392. <https://doi.org/10.1007/s12264-022-00938-2>
27. Igaz LM, Kwong LK, Lee EB, Chen-Plotkin A, Swanson E, Unger T, Malunda J, Xu Y, Winton MJ, Trojanowski JQ et al (2011) Dysregulation of the ALS-associated gene TDP-43 leads to neuronal death and degeneration in mice. *J Clin Invest* 121:726–738. <https://doi.org/10.1172/JCI44867>
28. Iguchi Y, Katsuno M, Niwa J, Takagi S, Ishigaki S, Ikenaka K, Kawai K, Watanabe H, Yamanaka K, Takahashi R et al (2013) Loss of TDP-43 causes age-dependent progressive motor neuron degeneration. *Brain* 136:1371–1382. <https://doi.org/10.1093/brain/awt029>
29. Jordan C, Friedrich V Jr, Dubois-Dalcq M (1989) In situ hybridization analysis of myelin gene transcripts in developing mouse spinal cord. *J Neurosci* 9:248–257. <https://doi.org/10.1523/jneurosci.09-01-00248.1989>
30. Kang SH, Li Y, Fukaya M, Lorenzini I, Cleveland DW, Ostrow LW, Rothstein JD, Bergles DE (2013) Degeneration and impaired regeneration of gray matter oligodendrocytes in amyotrophic lateral sclerosis. *Nat Neurosci* 16:571–579. <https://doi.org/10.1038/nn.3357>
31. Kim D, Langmead B, Salzberg SL (2015) HISAT: a fast spliced aligner with low memory requirements. *Nat Methods* 12:357–360. <https://doi.org/10.1038/nmeth.3317>
32. Kobayashi Y, Sano Y, Vannoni E, Goto H, Suzuki H, Oba A, Kawasaki H, Kanba S, Lipp HP, Murphy NP et al (2013) Genetic dissection of medial habenula-interpeduncular nucleus pathway function in mice. *Front Behav Neurosci* 7:17. <https://doi.org/10.3389/fnbeh.2013.00017>
33. Koeppen AH, Robitaille Y (2002) Pelizaeus-Merzbacher disease. *J Neuropathol Exp Neurol* 61:747–759. <https://doi.org/10.1093/jnen/61.9.747>
34. Lee Y, Morrison BM, Li Y, Lengacher S, Farah MH, Hoffman PN, Liu Y, Tsingalia A, Jin L, Zhang PW et al (2012) Oligodendroglia metabolically support axons and contribute to neurodegeneration. *Nature* 487:443–448. <https://doi.org/10.1038/nature11314>
35. Ling SC, Polymenidou M, Cleveland DW (2013) Converging mechanisms in ALS and FTD: disrupted RNA and protein homeostasis. *Neuron* 79:416–438. <https://doi.org/10.1016/j.neuron.2013.07.033>
36. Marinelli C, Bertalot T, Zusso M, Skaper SD, Giusti P (2016) Systematic review of pharmacological properties of the oligodendrocyte lineage. *Front Cell Neurosci* 10:27. <https://doi.org/10.3389/fncel.2016.00027>
37. Neumann M, Sampathu DM, Kwong LK, Truax AC, Micsenyi MC, Chou TT, Bruce J, Schuck T, Grossman M, Clark CM et al (2006) Ubiquitinated TDP-43 in frontotemporal lobar degeneration and amyotrophic lateral sclerosis. *Science* 314:130–133. <https://doi.org/10.1126/science.1134108>
38. Nishihira Y, Tan C-F, Onodera O, Toyoshima Y, Yamada M, Morita T, Nishizawa M, Kakita A, Takahashi H (2008) Sporadic amyotrophic lateral sclerosis: two pathological patterns shown by analysis of distribution of TDP-43-immunoreactive neuronal and glial cytoplasmic inclusions. *Acta Neuropathol* 116:169–182. <https://doi.org/10.1007/s00401-008-0385-z>
39. Niwa H, Yamamura K, Miyazaki J (1991) Efficient selection for high-expression transfectants with a novel eukaryotic vector. *Gene* 108:193–199. [https://doi.org/10.1016/0378-1119\(91\)90434-d](https://doi.org/10.1016/0378-1119(91)90434-d)
40. Niwa-Kawakita M, Abramowski V, Kalamirides M, Thomas G, Giovannini M (2000) Targeted expression of Cre recombinase to myelinating cells of the central nervous system in transgenic mice. *Genesis* 26:127–129
41. Nonneman A, Robberecht W, Van Den Bosch L (2014) The role of oligodendroglial dysfunction in amyotrophic lateral sclerosis. *Neurodegener Dis Manag* 4:223–239. <https://doi.org/10.2217/nmt.14.21>
42. Nutma E, van Gent D, Amor S, Peferoen LAN (2020) Astrocyte and oligodendrocyte cross-talk in the central nervous system. *Cells*. <https://doi.org/10.3390/cells9030600>
43. Oiwa K, Watanabe S, Onodera K, Iguchi Y, Kinoshita Y, Komine O, Sobue A, Okada Y, Katsuno M, Yamanaka K (2023) Monomerization of TDP-43 is a key determinant for inducing TDP-43 pathology in amyotrophic lateral sclerosis. *Sci Adv* 9:eadf6895. <https://doi.org/10.1126/sciadv.adf6895>
44. Pandey S, Shen K, Lee SH, Shen YA, Wang Y, Otero-Garcia M, Kotova N, Vito ST, Laufer BI, Newton DF et al (2022) Disease-associated oligodendrocyte responses across neurodegenerative diseases. *Cell Rep* 40:11189. <https://doi.org/10.1016/j.celrep.2022.111189>
45. Peferoen L, Kipp M, van der Valk P, van Noort JM, Amor S (2014) Oligodendrocyte-microglia cross-talk in the central nervous system. *Immunology* 141:302–313. <https://doi.org/10.1111/imm.12163>
46. Perez-Berlenga M, Wiersma VI, Zbinden A, De Vos L, Wagner U, Foglieni C, Mallona I, Betz KM, Clery A, Weber J et al (2023) Loss of TDP-43 oligomerization or RNA binding elicits distinct aggregation patterns. *EMBO J* 42:e111719. <https://doi.org/10.15252/emboj.2022111719>
47. Perteau M, Perteau GM, Antonescu CM, Chang TC, Mendell JT, Salzberg SL (2015) StringTie enables improved reconstruction of a transcriptome from RNA-seq reads. *Nat Biotechnol* 33:290–295. <https://doi.org/10.1038/nbt.3122>
48. Philips T, Bento-Abreu A, Nonneman A, Haecck W, Staats K, Geelen V, Hersmus N, Kusters B, Van Den Bosch L, Van Damme P et al (2013) Oligodendrocyte dysfunction in the pathogenesis of amyotrophic lateral sclerosis. *Brain* 136:471–482. <https://doi.org/10.1093/brain/aws339>
49. Polymenidou M, Lagier-Tourenne C, Hutt KR, Huelga SC, Moran J, Liang TY, Ling SC, Sun E, Wanczewicz E, Mazur C et al (2011) Long pre-mRNA depletion and RNA missplicing contribute to neuronal vulnerability from loss of TDP-43. *Nat Neurosci* 14:459–468. <https://doi.org/10.1038/nn.2779>
50. Prasad A, Bharathi V, Sivalingam V, Girdhar A, Patel BK (2019) Molecular mechanisms of TDP-43 misfolding and pathology in amyotrophic lateral

- sclerosis. *Front Mol Neurosci* 12:25. <https://doi.org/10.3389/fnmol.2019.00025>
51. Prusiner SB, Woerman AL, Mordes DA, Watts JC, Rampersaud R, Berry DB, Patel S, Oehler A, Lowe JK, Kravitz SN et al (2015) Evidence for alpha-synuclein prions causing multiple system atrophy in humans with parkinsonism. *Proc Natl Acad Sci USA* 112:E5308–5317. <https://doi.org/10.1073/pnas.1514475112>
  52. Quinlan AR, Hall IM (2010) BEDTools: a flexible suite of utilities for comparing genomic features. *Bioinformatics* 26:841–842. <https://doi.org/10.1093/bioinformatics/btq033>
  53. Ricketts T, McGoldrick P, Fratta P, de Oliveira HM, Kent R, Phatak V, Brandner S, Blanco G, Greensmith L, Acevedo-Arozena A et al (2014) A nonsense mutation in mouse Tardbp affects TDP43 alternative splicing activity and causes limb-clasping and body tone defects. *PLoS ONE* 9:e85962. <https://doi.org/10.1371/journal.pone.0085962>
  54. Rohan Z, Matej R, Rusina R, Kovacs GG (2014) Oligodendroglial response in the spinal cord in TDP-43 proteinopathy with motor neuron involvement. *Neurodegener Dis* 14:117–124. <https://doi.org/10.1159/000362929>
  55. Shiota C, Mikoshiba K (1990) *In situ* hybridization with cDNA probes its application to the detection of mRNAs for myelin proteins (PLP AND MBP) in mouse brain sections. *Acta Histochemica et Cytochemica* 23:297–306. <https://doi.org/10.1267/ahc.23.297>
  56. Soriano P (1999) Generalized lacZ expression with the ROSA26 Cre reporter strain. *Nat Genet* 21:70–71. <https://doi.org/10.1038/5007>
  57. Sreedharan J, Blair IP, Tripathi VB, Hu X, Vance C, Rogelj B, Ackerley S, Durnall JC, Williams KL, Buratti E et al (2008) TDP-43 mutations in familial and sporadic amyotrophic lateral sclerosis. *Science* 319:1668–1672. <https://doi.org/10.1126/science.1154584>
  58. Suzuki H, Shibagaki Y, Hattori S, Matsuoaka M (2015) Nuclear TDP-43 causes neuronal toxicity by escaping from the inhibitory regulation by hnRNPs. *Hum Mol Genet* 24:1513–1527. <https://doi.org/10.1093/hmg/ddu563>
  59. Tan RH, Ke YD, Ittner LM, Halliday GM (2017) ALS/FTLD: experimental models and reality. *Acta Neuropathol* 133:177–196. <https://doi.org/10.1007/s00401-016-1666-6>
  60. Taylor JP, Brown RH Jr, Cleveland DW (2016) Decoding ALS: from genes to mechanism. *Nature* 539:197–206. <https://doi.org/10.1038/nature20413>
  61. Tollervey JR, Curk T, Rogelj B, Briese M, Cereda M, Kayikci M, Konig J, Hortobagyi T, Nishimura AL, Zupunski V et al (2011) Characterizing the RNA targets and position-dependent splicing regulation by TDP-43. *Nat Neurosci* 14:452–458. <https://doi.org/10.1038/nn.2778>
  62. Tsuboguchi S, Nakamura Y, Ishihara T, Kato T, Sato T, Koyama A, Mori H, Koike Y, Onodera O, Ueno M (2023) TDP-43 differentially propagates to induce antero- and retrograde degeneration in the corticospinal circuits in mouse focal ALS models. *Acta Neuropathol* 146:611–629. <https://doi.org/10.1007/s00401-023-02615-8>
  63. Tsujii H, Inoue I, Takeuchi M, Furuya A, Yamakage Y, Watanabe S, Koike M, Hattori M, Yamanaka K (2017) TDP-43 accelerates age-dependent degeneration of interneurons. *Sci Rep* 7:14972. <https://doi.org/10.1038/s41598-017-14966-w>
  64. Tung VW, Burton TJ, Dababneh E, Quail SL, Camp AJ (2014) Behavioral assessment of the aging mouse vestibular system. *J Vis Exp*. <https://doi.org/10.3791/51605>
  65. Van Deerlin VM, Leverenz JB, Bekris LM, Bird TD, Yuan W, Elman LB, Clay D, Wood EM, Chen-Plotkin AS, Martinez-Lage M et al (2008) TARDBP mutations in amyotrophic lateral sclerosis with TDP-43 neuropathology: a genetic and histopathological analysis. *Lancet Neurol* 7:409–416. [https://doi.org/10.1016/S1474-4422\(08\)70071-1](https://doi.org/10.1016/S1474-4422(08)70071-1)
  66. Wagner GP, Kin K, Lynch VJ (2012) Measurement of mRNA abundance using RNA-seq data: RPKM measure is inconsistent among samples. *Theory Biosci* 131:281–285. <https://doi.org/10.1007/s12064-012-0162-3>
  67. Wang J, Ho WY, Lim K, Feng J, Tucker-Kellogg G, Nave KA, Ling SC (2018) Cell-autonomous requirement of TDP-43, an ALS/FTD signature protein, for oligodendrocyte survival and myelination. *Proc Natl Acad Sci USA* 115:E10941–E10950. <https://doi.org/10.1073/pnas.1809821115>
  68. Watanabe S, Kaneko K, Yamanaka K (2013) Accelerated disease onset with stabilized familial amyotrophic lateral sclerosis (ALS)-linked mutant TDP-43 proteins. *J Biol Chem* 288:3641–3654. <https://doi.org/10.1074/jbc.M112.433615>
  69. Watanabe S, Oiwa K, Murata Y, Komine O, Sobue A, Endo F, Takahashi E, Yamanaka K (2020) ALS-linked TDP-43(M337V) knock-in mice exhibit splicing deregulation without neurodegeneration. *Mol Brain* 13:8. <https://doi.org/10.1186/s13041-020-0550-4>
  70. White MA, Kim E, Duffy A, Adalbert R, Phillips BU, Peters OM, Stephenson J, Yang S, Massenzio F, Lin Z et al (2018) TDP-43 gains function due to perturbed autoregulation in a Tardbp knock-in mouse model of ALS-FTD. *Nat Neurosci* 21:552–563. <https://doi.org/10.1038/s41593-018-0113-5>
  71. Wils H, Kleinberger G, Janssens J, Pereson S, Joris G, Cuijt I, Smits V, Ceuterick-de Groote C, Van Broeckhoven C, Kumar-Singh S (2010) TDP-43 transgenic mice develop spastic paralysis and neuronal inclusions characteristic of ALS and frontotemporal lobar degeneration. *Proc Natl Acad Sci USA* 107:3858–3863. <https://doi.org/10.1073/pnas.0912417107>
  72. Xu YF, Zhang YJ, Lin WL, Cao X, Stetler C, Dickson DW, Lewis S, Petrucelli L (2011) Expression of mutant TDP-43 induces neuronal dysfunction in transgenic mice. *Mol Neurodegener* 6:73. <https://doi.org/10.1186/1750-1326-6-73>
  73. Yazawa I, Giasson BI, Sasaki R, Zhang B, Joyce S, Uryu K, Trojanowski JQ, Lee VM (2005) Mouse model of multiple system atrophy alpha-synuclein expression in oligodendrocytes causes glial and neuronal degeneration. *Neuron* 45:847–859. <https://doi.org/10.1016/j.neuron.2005.01.032>
  74. Yokoseki A, Shiga A, Tan CF, Tagawa A, Kaneko H, Koyama A, Eguchi H, Tsujino A, Ikeuchi T, Kakita A et al (2008) TDP-43 mutation in familial amyotrophic lateral sclerosis. *Ann Neurol* 63:538–542. <https://doi.org/10.1002/ana.21392>

## Publisher's Note

Springer Nature remains neutral with regard to jurisdictional claims in published maps and institutional affiliations.